J. Fluid Mech. (2009), *vol.* 629, *pp.* 311–342.
doi:10.1017/S0022112009006387 Printed in the United Kingdom

Grain sorting effects on the formation of tidal sand waves

TOMAS VAN OYEN AND PAOLO BLONDEAUX†

Department of Civil, Environmental and Architectural Engineering, University of Genoa, Via Montallegro 1, 16145 Genova, Italy

(Received 29 April 2008 and in revised form 27 January 2009)

A model is developed to investigate the process which leads to the formation of sand waves in shallow tidal seas characterized by a heterogeneous sea bed composition. The main goal of the analysis is the evaluation of the effects that a graded sediment has on the formation of the bottom forms and the investigation of the sorting process induced by the growth of the bottom forms. The analysis is based on the study of the stability of the flat bed configuration, i.e. small amplitude perturbations are added to the flat bottom and a linear analysis of their time development is made. For an oscillatory tidal current dominated by one tidal constituent, the results show that the graded sediment can stabilize or destabilize the flat bottom configuration with respect to the uniform sediment case, depending on the standard deviation σ^* of the grain size distribution and on the ratio $\hat{r}$ between the horizontal tidal excursion and the water depth. For moderate values of $\hat{r}$, i.e. values just larger than the critical value for which the sediment is moved and sand waves appear, the presence of a sand mixture stabilizes the flat bed. On the other hand, for large values of $\hat{r}$, the mixture has a destabilizing effect. In both cases the effect that a sand mixture has on the stability of the flat bed configuration is relatively small. Moreover, for moderate values of $\hat{r}$, the fine fraction of the mixture tends to pile up at the crests of the bottom forms while the coarse fraction moves towards the troughs. For large values of $\hat{r}$, the grain size distribution depends on the value of σ^*. The results are physically interpreted and provide a possible explanation of the apparently conflicting field observations of the grain size distribution along the sand wave profile, carried out in the North Sea.

1. Introduction

Recently, theoretical models have been developed to analyse the effects of graded sediments on the formation of large-scale tidal bed forms (e.g. sand banks, tidal sand ridges, sand waves).

These studies have been motivated by field surveys which show that quite often the sea bottom is made up of sediment mixtures characterized by a wide probability density distribution. Moreover, field observations reveal spatial variations in the mean grain size along tidal bed forms, indicating sorting processes (Terwindt 1971; Swift *et al.* 1978; Antia 1996; Van Lancker & Jacobs 2000; Roos *et al.* 2007*a*). As pointed out by Walgreen, De Swart & Calvete (2004), a well-documented example is the Middelkerke Bank along the Belgian coast (Houthuys *et al.* 1994; Lanckneus, De Moor & Stolk 1994; Vincent, Stolk & Porter 1998), where the distribution of the

† Email address for correspondence: blx@dicat.unige.it

mean grain size shows an accumulation of the coarser sediment on the crests and of the finer sediment in the troughs. Data gathered from the more seaward located Kwinte Bank (Gao *et al.* 1994) indicate a similar grain size pattern and variations in the mean grain size are found also for the more onshore located coastal banks (Van Lancker 1999). As described by Roos *et al.* (2007*a*), an overview of the grain size patterns over tidal sand waves in the southern part of the North Sea shows less persistent trends. Indeed, at some locations (site 1, near Zandvoort; site 2, offshore of Egmond aan Zee; site 4, near Hoek van Holland) the medium grain size at the crests is coarser than that at the troughs but at other locations (site 3, on Brown Bank; site 5, on Thorton Bank) the sediment is coarser at the troughs. Note that the site numbers correspond to those shown in figure 16. Similar field data are described in Terwindt (1971) and Van Lancker & Jacobs (2000).

To investigate the formation of tidal sand ridges, Walgreen *et al.* (2004) considered the time development of bottom perturbations on an along-shore uniform continental shelf. A semi-infinite domain is introduced, which is bounded on the landward side by the shoreface and is characterized by a bathymetry that has a constant slope close to the coast while the water depth becomes constant further offshore. The morphodynamic system is driven by an oscillatory tidal current which is assumed to be parallel to the coastline. In this case the growth of the bottom perturbations leads to the formation of tidal sand ridges and the results obtained by Walgreen *et al.* indicate that the growth and the migration rate of the bottom forms increase if a bimodal mixture replaces a well-sorted sediment, even though the wavelength of the ridges remains practically unchanged. Moreover, for a symmetrical tidal current, the coarse sediment is found to pile up at the crests of the ridges while the fine sediment is found in the troughs.

Roos *et al.* (2007*b*) investigated the effects of a graded sediment on the growth of the large-scale bottom forms (sand banks) which are generated by tidal currents on a continental shelf characterized by an average constant water depth. Similar to the results of Walgreen *et al.* (2004), the results obtained by Roos *et al.* (2007*b*) show that the growth rate of the bottom forms increases, if compared to the case of the uniform sediment. However, the preferred wavelength and the ridge orientation remain unchanged. Moreover, the coarse sediment fraction tends to accumulate at the bank crests.

During the last decade a lot of morphodynamic models have been developed to investigate and simulate sand wave dynamics because of their strong interference with human activities in shelf seas (Besio *et al.* 2008). However, a large number of these models (a.o. Hulscher 1996; Gerkema 2000; Besio, Blondeaux & Frisina 2003; Besio, Blondeaux & Vittori 2006) consider a uniform homogeneous sediment. As previously described, field observations at various locations in the North Sea indicate that the mean grain size varies along the bed form profile (Schüttenhelm 2002; Passchier & Kleinhans 2005) and laboratory experiments (Foti & Blondeaux 1995*b*) indicate that the grain sorting processes can affect the characteristics and dynamics of bottom forms. Hence, recently, Roos *et al.* (2007*a*) have investigated the time development of sand waves which appear in a sediment mixture. Roos *et al.* used a numerical model based on that of van den Berg & Van Damme (2005) extending it by introducing (i) the active layer approach of Hirano (1971), (ii) a fractional calculation of the sediment transport and (iii) hiding/exposure effects. The numerical results indicate that, starting from a sinusoidal shape, sand waves evolve towards an equilibrium profile which has peaked crests and flattened troughs. The growth of sand waves is accompanied by a continuous redistribution of the fine and coarse sediments and the concentration of

the coarse grains increases at the crests while the sediment in the troughs remains well mixed. Even though the model is unable to account for the variation of the length of the bottom forms, it takes into account nonlinear effects and can describe the growth of the amplitude of sand waves till large values are attained. In this respect, the model of Roos *et al.* is a powerful tool to analyse the morphodynamic process under investigation. However, the model is computationally expensive and the investigation of the parameter space implies high costs. For example, it is difficult to determine the effects that a sediment mixture has on the wavelength of the most unstable bottom mode.

In the following we describe a model able to investigate the initial stage of sand wave formation when a heterogeneous sediment is considered. The study is aimed at describing the effects that a sediment mixture has on the growth of tidal sand waves and at investigating the grain size distribution along the bed forms to reveal the basic mechanisms controlling the sorting process. The analysis is based on the study of the stability of the flat bottom, i.e. small bottom perturbations of the flat configuration are considered and a linear analysis of their growth is made. To describe the hydrodynamics and the morphodynamics of the tidal sea, the model proposed by Blondeaux & Vittori (2005*a*, *b*) is used and modified to take into account the presence of a graded sediment.

The procedure used in the rest of the paper is as follows. In the next section we formulate the hydrodynamic and morphodynamic problems. In § 3, the interaction of the tidal current with an arbitrary bottom perturbation is studied and the conditions leading to the appearance of sand waves are determined. Moreover, the grain sorting process along the bottom forms is analysed. Next, the results are described and physically interpreted in § 4. In § 5, the theoretical predictions are compared with field observations carried out in the North Sea. Finally, some conclusions are drawn in § 6.

2. Model formulation

A local model is used to consider the flow-topography interaction in a shallow tidal sea. The flow domain consists of a constant average water depth h_0^* and is horizontally unbounded (hereinafter a star denotes dimensional quantities). First, we formulate the morphodynamic problem, in particular we specify how the model accounts for the heterogeneity of the sediment mixture. Then the hydrodynamic problem is described.

2.1. *Morphodynamic problem*

A tidal sea the sea bed of which is assumed to consist of a cohesionless sediment mixture of constant density ρ_s^* and porosity p_{or} is considered. The sediment mixture is described by introducing a finite number N of distinct grain size classes. Each grain size class lays within the sand region and is characterized by a grain size diameter d_n^* with associated volume fraction p_n ($n = 1, 2, \ldots, N$). Thus, the probability density function $p^*(d^*)$ of the heterogeneous sediment is given by

$$p^*(d^*) = \sum_{n=1}^{N} p_n \delta(d^* - d_n^*), \tag{2.1}$$

where δ is the Dirac function. The values of p_n may vary in both space and time, but the sum of all grain size fractions must equal 1 everywhere:

$$\sum_{n=1}^{N} p_n = 1. \tag{2.2}$$

The sediment is assumed to be characterized by a mean grain size d^*_{mean} and a standard deviation σ^* given by

$$d^*_{mean} = \sum_{n=1}^{N} d^*_n p_n, \quad \sigma^{*2} = \sum_{n=1}^{N} (d^*_n - d^*_{mean})^2 p_n, \tag{2.3}$$

and the effects of higher moments of the sediment distribution (e.g. skewness, kurtosis) are neglected.

The aim of the work is to evaluate the time development of small amplitude perturbations superimposed to the flat bottom configuration, in order to determine the conditions leading to the appearance of sand waves. The stability analysis of the flat bed has already been made considering a uniform sediment (e.g. Hulscher 1996; Gerkema 2000; Besio *et al.* 2003; Besio *et al.* 2006). Presently, we consider the behaviour of the perturbations for a sediment mixture, thereby being interested in the sorting process induced by the incipient growth of sand waves and in the stabilizing/destabilizing effects that a graded sediment has on the formation of these bottom forms.

The transport of bed material is associated with small-scale fluctuations in the bed elevation induced by the moving sediment grains or by the migration of small bed forms (ripples). As pointed out by Parker (2007), these bed fluctuations are essential to the understanding of the transport of a sediment mixture. Indeed, for a sediment grain in the bed to be entrained into motion, it must be exposed to the action of the fluid. Therefore, the higher the elevation of the grain, the higher is the probability that it is entrained. The simplest reasonable approximation of the probability of entrainment per unit time of a grain as a function of elevation in the bed is a step function, such that the probability of erosion of a grain per unit time has a constant value in an 'exchange' or 'active' layer of thickness L^*_a near the bed surface, and vanishes below this layer. This approximation was first introduced by Hirano (1971). The value of L^*_a is either of the order of magnitude of the size of the sediment when the sea bottom is flat or of the order of magnitude of the ripple height z^*_r when small-scale bed forms are generated. In the present case, since sea ripples are supposed to be present, we assume $L^*_a = z^*_r$ where z^*_r is a constant value.

Let the fractions in the size distribution in the active layer be denoted as $p_{a,n}$. Note that $p_{a,n}$ might be functions of time t^* and horizontal coordinates x^* and y^*, but they cannot be functions of the upward normal coordinate z^* because the 'active' layer is assumed to be instantaneously well mixed. The size fractions in the substrate below the active layer are denoted by $p_{s,n}$. In general, $p_{s,n}$ can be a function of space, defining the stratigraphy of the deposit. However, $p_{s,n}$ are independent of t^* because they are assumed to be below the level of bed fluctuations. Figure 1 presents a side view of the water column and the active layer concept.

Following previous studies of sand wave formation carried out considering both a homogeneous and a heterogeneous sediment (Hulscher 1996; Gerkema 2000; Besio *et al.* 2003; Roos *et al.* 2007*a*), the suspended load is assumed to provide a negligible contribution to the total sediment transport rate. Therefore, the analysis is valid for a relatively coarse sediment and weak tidal currents such that the turbulent eddies are unable to pick up the sediment from the bottom and carry it into suspension.

Let $(Q^*_{x,n}, Q^*_{y,n})$ denote the volumetric flux per unit width of grains of size d^*_n in the x^* and y^* directions, respectively. Within the bed, each grain size class n should satisfy sediment continuity. This conservation law relates local changes in both bed

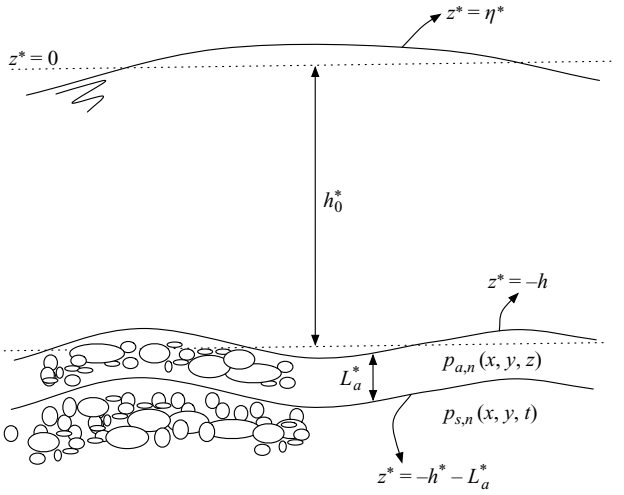

FIGURE 1. Side view of the water column and the active layer concept. The thickness of the active layer and the variation of the free surface are exaggerated for the clearness of the sketch.

level and grain size distribution,

$$-p_{i,n}\frac{\partial(h^* + L_a^*)}{\partial t^*} + \frac{\partial(L_a^* p_{a,n})}{\partial t^*} = -\frac{1}{(1 - p_{or})}\left[\frac{\partial Q_{x,n}^*}{\partial x^*} + \frac{\partial Q_{y,n}^*}{\partial y^*}\right]. \tag{2.4}$$

In the above relation, $z^* = -h^*$ denotes the elevation of the bottom, so that the elevation of the interface between the active layer and the substrate is given by $z^* = -h^* - L_a^*$ ($z^* = 0$ is assumed to describe the mean water level). Moreover, $p_{i,n}$ denote the size fractions of the material exchanged between the active layer and the substrate as the bed aggrades or degrades ($p_{i,n} = p_{a,n}$ if $\partial(h^* + L_a^*)/\partial t^* < 0$ and $p_{i,n} = p_{s,n}$ if $\partial(h^* + L_a^*)/\partial t^* \geqslant 0$). The first term on the left-hand side of (2.4) represents the bottom changes and the second describes changes in the sediment distribution in the active layer.

By summing all grain size fractions, the individual sediment continuity equations (2.4) add up to a single equation relating the bed evolution to the divergence of the total sediment transport rate:

$$\frac{\partial h^*}{\partial t^*} = \frac{1}{(1 - p_{or})}\left[\frac{\partial Q_{x,tot}^*}{\partial x^*} + \frac{\partial Q_{y,tot}^*}{\partial y^*}\right], \tag{2.5}$$

where

$$(Q_{x,tot}^*, Q_{y,tot}^*) = \sum_{n=1}^{N}(Q_{x,n}^*, Q_{y,n}^*). \tag{2.6}$$

As previously pointed out, the suspended load is assumed to be negligible and only transport of sediment close to the bed is considered. The bed load is evaluated by means of the approach proposed by Van Rijn (1991), corrected to account for the gravity effects which move the sediment towards the troughs of the bottom waviness (Besio *et al.* 2006).

For a specific grain size within a sediment mixture, two further corrections should be introduced. First, $p_{a,n}$ corrects for the availability of grains of size d_n^* in the mixture. Second, hiding/exposure effects should be included, represented by the function H which appears in the definition of the critical value of the Shields parameter (Egiazaroff 1965). These effects should be taken into account since the transport of fine grains is hindered as they are protected by the surrounding coarser grains. Conversely, the transport of coarse grains is enhanced as, in the presence of finer grains, they are more exposed and thus transported more easily by the flow. Therefore,

$$(Q_{x,n}^*, Q_{y,n}^*) = p_{a,n}\left(Q_{x,n}^{(u)*}, Q_{y,n}^{(u)*}\right), \tag{2.7}$$

where the bed-load transport rate per unit fraction is given by the sum of two contributions:

$$\left(Q_{x,n}^{(u)*}, Q_{y,n}^{(u)*}\right) = \left(Q_{B,x,n}^{(u)*}, Q_{B,y,n}^{(u)*}\right) + \left(Q_{P,x,n}^{(u)*}, Q_{P,y,n}^{(u)*}\right). \tag{2.8}$$

To evaluate the former, which is the sediment transport rate per unit fraction over a horizontal bed, we use the approach of Van Rijn (1991):

$$\left(Q_{B,x,n}^{(u)*}, Q_{B,y,n}^{(u)*}\right) = \sqrt{(\rho_s^*/\rho^* - 1)g^*(d_n^*)^3}\frac{0.25}{R_{p,n}^{0.2}}\left(\frac{\theta_n - \theta_{crit,n}}{\theta_{crit,n}}\right)^{1.5}\frac{(\theta_{x,n}, \theta_{y,n})}{\sqrt{\theta_n}}. \tag{2.9}$$

Of course (2.9) can be used to evaluate the sediment transport rate only when θ_n is larger than $\theta_{crit,n}$; otherwise the sediment transport rate vanishes. In (2.9), ρ^* is the sea water density and $R_{p,n}$ is the Reynolds number of the sand fraction characterized by a grain size d_n^* ($R_{p,n} = \sqrt{(\rho_s^*/\rho^* - 1)g^*(d_n^*)^3}/\nu^*$, ν^* being the kinematic viscosity of the sea water). The sediment transport rate due to the slope of the bed, which is the second contribution appearing in (2.8), is given by

$$\left(Q_{P,x,n}^{(u)*}, Q_{P,y,n}^{(u)*}\right) = -Q_{B,n}^{(u)*}\mathbf{G}\nabla h^*. \tag{2.10}$$

In (2.10), $\mathbf{G}$ is a dimensionless second-order two-dimensional tensor which, following Kovacs & Parker (1994) and Seminara (1998), can be written in the form

$$G_{ss} = -\frac{0.07}{Q_{B,n}^{(u)*}}\frac{dQ_{B,n}^{(u)*}}{d\theta_n}, \quad G_{sn} = G_{ns} = 0, \quad G_{nn} = -\frac{0.55}{\sqrt{\theta_n}}, \tag{2.11}$$

where (s, n) is an intrinsic orthogonal coordinate system, with s aligned with the bottom stress. Finally, $(\theta_{x,n}, \theta_{y,n})$ are the x^* and y^* components of the Shields parameter due to the tidal current defined by

$$(\theta_{x,n}, \theta_{y,n}) = \frac{(\tau_x^*, \tau_y^*)}{(\rho_s^* - \rho^*)g^*d_n^*}, \tag{2.12}$$

where (τ_x^*, τ_y^*) are the dimensional shear stress components, which can be evaluated by means of the constitutive law. Note that the components of the Shields parameter $(\theta_{x,n}, \theta_{y,n})$ and the sediment parameter $R_{p,n}$ in the formulae for the sediment transport rate are evaluated for each grain size class, thus accounting for the reduced mobility of a coarser grain with respect to a finer grain.

As recently pointed out by Colombini (2004), to study the time development of bottom perturbations, the shear stress exerted by the fluid on the sediments moving close to the bed should be evaluated at top of the so-called bed-load layer. In other words, it is the shear stress which is present at some distance from the bed and not the shear stress at the bed which should be used to estimate the bed-load discharge. Therefore, as in Colombini (2004) and Cherlet *et al.* (2007), a new parameter is

introduced in the analysis, namely the thickness of the bed-load layer h_b^*. Moreover, as in Cherlet *et al.* (2007), because of the supposed presence of small-scale ripples of height z_r^*, it is assumed that

$$h_b^* = z_r^* \left[1 + 1.3 \left(\frac{\theta_n - \theta_{crit,mean}}{\theta_{crit,mean}} \right)^{0.55} \right]. \tag{2.13}$$

The critical value $\theta_{crit,n}$ of the Shields parameter, which appears into (2.9) and characterizes the grains with size equal to d_n^*, is written as function of the critical Shields parameter of the mean grain size and of the ratio d_n^*/d_{mean}^* (Egiazaroff 1965; Ashida & Michiue 1972):

$$\theta_{crit,n} = \theta_{crit,mean} H \left(\frac{d_n^*}{d_{mean}^*} \right), \tag{2.14}$$

where

$$H \left(\frac{d_n^*}{d_{mean}^*} \right) = 0.843 \frac{d_{mean}^*}{d_n^*} \quad \text{if} \quad \frac{d_n^*}{d_{mean}^*} \leqslant 0.4, \tag{2.15}$$

$$H \left(\frac{d_n^*}{d_{mean}^*} \right) = \left[\frac{\log(19)}{\log \left(19 \dfrac{d_n^*}{d_{mean}^*} \right)} \right]^2 \quad \text{if} \quad \frac{d_n^*}{d_{mean}^*} > 0.4. \tag{2.16}$$

The critical Shields parameter of the mean grain size, used in (2.14), is evaluated by means of the relationship proposed by Brownlie (1981) which reads

$$\theta_{crit,mean} = 0.22 R_{p,mean}^{-0.6} + 0.06 \exp\left(-17.77 R_{p,mean}^{-0.6}\right). \tag{2.17}$$

Introducing the following dimensionless variables

$$(x, y, z) = \frac{(x^*, y^*, z^*)}{h_0^*}, \quad t = t^* \omega^*, \tag{2.18}$$

$$h = \frac{h^*}{h_0^*}, \quad L_a = \frac{L_a^*}{h_0^*}, \quad (Q_{x,n}, Q_{y,n}) = \frac{(Q_{x,n}^*, Q_{y,n}^*)}{\sqrt{(\rho_s^*/\rho^* - 1) g^* (d_{mean,0}^*)^3}},$$

(ω^* denotes the angular frequency of the forcing tide and $d_{mean,0}^*$ is the initial mean grain size of the mixture which is assumed to be constant in space), the morphodynamic problem is posed by

$$-p_{i,n} \frac{\partial (h + L_a)}{\partial t} + \frac{\partial (L_a p_{a,n})}{\partial t} = -\beta \left[\frac{\partial Q_{x,n}}{\partial x} + \frac{\partial Q_{y,n}}{\partial y} \right], \tag{2.19}$$

and

$$\frac{\partial h}{\partial t} = \beta \left[\frac{\partial Q_{x,tot}}{\partial x} + \frac{\partial Q_{y,tot}}{\partial y} \right], \tag{2.20}$$

where the dimensionless parameter β is equal to

$$\beta = \frac{1}{(1 - p_{or})} \frac{d_{mean,0}}{\sqrt{\Psi_{mean}}}, \tag{2.21}$$

with

$$d_{mean,0} = \frac{d_{mean,0}^*}{h_0^*}, \quad \Psi_{mean} = \frac{(\omega^* h_0^*)^2}{(\rho_s^*/\rho^* - 1) g^* d_{mean,0}^*}. \tag{2.22}$$

Since in the present problem L_a^* is assumed to be constant and equal to the ripple height z_r^*, it follows that $\partial L_a^*/\partial t = 0$ and (2.19) becomes

$$-p_{i,n}\frac{\partial h}{\partial t} + L_a\frac{\partial p_{a,n}}{\partial t} = -\beta\left[\frac{\partial Q_{x,n}}{\partial x} + \frac{\partial Q_{y,n}}{\partial y}\right]. \tag{2.23}$$

At this stage, it is elucidating to analyse the order of magnitude of the different terms appearing in (2.20) and (2.23). Taking into account that the active layer thickness is of the order of a few centimetres and the average water depth is of the order of tens of metres, the term $L_a\partial p_{a,n}/\partial t$ is found to be of order 10^{-4}. Furthermore, considering that the mean grain size is of the order of a few millimetres and considering a tidal flow dominated by the semidiurnal component, β turns out to be also of the order 10^{-4}. Consequently, the terms on the right-hand side of (2.20) and (2.23) are of order 10^{-4}. Then, (2.20) suggests that either the bed evolves on a morphodynamic time coordinate $T = \beta t$, which is much longer than the tidal period, or the bed changes are very small. Furthermore, since $L_a\partial p_{a,n}/\partial t$ is approximately of the same order of magnitude as the term related to the convergence or divergence of the sediment transport, the equation obtained by eliminating $\partial h/\partial t$ from (2.23) using (2.20) suggests that the bed composition changes on both the tidal and the morphodynamic time scales.

To proceed further, it is necessary to evaluate the bed shear stress. Therefore, in the next part, the hydrodynamic problem is specified.

2.2. *Hydrodynamic problem*

As pointed out in § 1, the morphodynamics is forced by a tidal current which is assumed to be dominated by one main constituent of angular frequency ω^*. The maximum value of the depth-averaged fluid velocity during the tidal cycle is denoted by U_0^*. As discussed in Blondeaux & Vittori (2005*a*, *b*), the hydrodynamic problem is posed by continuity and momentum equations where the Coriolis contributions related to the Earth's rotation (Ω^* is the angular velocity of the Earth's rotation and ϕ_0 is the local latitude) are taken into account because they affect the velocity profile of the tidal current over the flat sea bottom. However, as pointed out by Gerkema (2000) and Besio *et al.* (2006), when the interaction of a tidal current with a bottom waviness characterized by a wavelength of the order of hundreds of metres is considered, the terms related to inertia and Coriolis effects can be neglected. Therefore, Coriolis terms are retained when the tidal current over a flat bed is determined but they are neglected when the flow over the bottom perturbations is evaluated. Furthermore, the flow regime is assumed to be turbulent and viscous effects are neglected. The Boussinesq hypothesis is used to model Reynolds stresses and a scalar kinematic eddy viscosity ν_T^* is introduced.

On defining the following dimensionless variables

$$(u, v, w) = (u^*, v^*, w^*)/U_0^*\ ,\ \ p = p^*/\rho^*\omega^* h_0^* U_0^*, \tag{2.24}$$

(p^* denotes the pressure and (u^*, v^*, w^*) are the velocity components along the x^*, y^* and z^* axes, respectively) the flow equations read

$$\frac{\partial u}{\partial x} + \frac{\partial v}{\partial y} + \frac{\partial w}{\partial z} = 0, \tag{2.25}$$

$$\frac{\partial u}{\partial t} + \hat{r}\left[u\frac{\partial u}{\partial x} + v\frac{\partial u}{\partial y} + w\frac{\partial u}{\partial y}\right] = -\frac{\partial p}{\partial x} + \hat{\delta}^2\left\{\frac{\partial}{\partial x}\left[2\nu_T\frac{\partial u}{\partial x}\right]\right.$$
$$\left. + \frac{\partial}{\partial y}\left[\nu_T\left(\frac{\partial u}{\partial y} + \frac{\partial v}{\partial x}\right)\right] + \frac{\partial}{\partial z}\left[\nu_T\left(\frac{\partial u}{\partial z} + \frac{\partial w}{\partial x}\right)\right]\right\} - 2\Omega[\cos(\phi_0)w - \sin(\phi_0)v], \tag{2.26}$$

$$\frac{\partial v}{\partial t}+\hat{r}\left[u\frac{\partial v}{\partial x}+v\frac{\partial v}{\partial y}+w\frac{\partial v}{\partial y}\right]=-\frac{\partial p}{\partial y}+\hat{\delta}^2\left\{\frac{\partial}{\partial x}\left[\nu_T\left(\frac{\partial u}{\partial y}+\frac{\partial v}{\partial x}\right)\right]+\frac{\partial}{\partial y}\left[2\nu_T\frac{\partial v}{\partial y}\right]+\frac{\partial}{\partial z}\left[\nu_T\left(\frac{\partial v}{\partial z}+\frac{\partial w}{\partial y}\right)\right]\right\}-2\Omega\sin(\phi_0)u, \quad (2.27)$$

$$\frac{\partial w}{\partial t}+\hat{r}\left[u\frac{\partial w}{\partial x}+v\frac{\partial w}{\partial y}+w\frac{\partial w}{\partial y}\right]=-\frac{g^*}{U_0^*\omega^*}-\frac{\partial p}{\partial z}+\hat{\delta}^2\left\{\frac{\partial}{\partial x}\left[\nu_T\left(\frac{\partial u}{\partial z}+\frac{\partial w}{\partial x}\right)\right]+\frac{\partial}{\partial y}\left[\nu_T\left(\frac{\partial v}{\partial z}+\frac{\partial w}{\partial y}\right)\right]+\frac{\partial}{\partial z}\left[2\nu_T\frac{\partial w}{\partial z}\right]\right\}+2\Omega\cos(\phi_0)u, \quad (2.28)$$

where the kinematic eddy viscosity ν_T^* is written as the product $\nu_{T0}^*\nu_T$ in which the constant ν_{T0}^* is dimensional and provides the order of magnitude of the eddy viscosity while $\nu_T=\nu_T(x, y, z, t)$ is a dimensionless function (of order 1) describing the spatial and temporal variations of the turbulence structure. In (2.26)–(2.28), two dimensionless parameters appear which are denoted by $\hat{r}$ and $\hat{\delta}$, respectively:

$$\hat{r}=\frac{U_0^*}{\omega^* h_0^*}, \quad \hat{\delta}=\frac{\sqrt{\nu_{T0}^*/\omega^*}}{h_0^*}. \quad (2.29)$$

The ratio $\hat{r}$ between the amplitude of horizontal fluid displacement oscillations and the local depth is the Keulegan–Carpenter number of the phenomenon. Furthermore, $\hat{\delta}$ is the ratio between the thickness of the viscous bottom boundary layer and the local depth. Finally, Ω is the ratio between the angular velocity of the Earth's rotation and the angular frequency of the tidal wave.

The hydrodynamic problem needs appropriate boundary conditions. At the free surface, described by $z=\eta(x, y, t)$, wind stresses are assumed to be negligible and the dynamic boundary conditions force the vanishing of the shear stresses and of the relative pressure. Moreover, the kinematic boundary condition is forced. Finally, the velocity is forced to vanish at a distance from the sea bed equal to a fraction $1/\chi$ of the dimensionless roughness z_r equal to z_r^*/h_0^*, z_r^* being the size of the bottom roughness. As the flow induced by the tide propagation can be assumed to be quasi-steady, the constant χ is chosen equal to 29.8 based on an analysis of data of steady velocity profiles (Fredsøe & Deigaard 1992).

The problem can be closed once a model for the eddy viscosity ν_T^* is given. The eddy viscosity ν_T^* is assumed to be time independent and given by

$$\nu_T^*=k\frac{U_0^* h_0^*}{\mathscr{C}}F(\xi). \quad (2.30)$$

In (2.30), k is the Von Karman constant ($k=0.4$) and the eddy viscosity is assumed to be proportional to the time average of the local friction velocity and to the local depth h_0^*. Then, the average friction velocity is related to U_0^* by introducing the friction factor $\mathscr{C}$. Since the Reynolds number of the flow is assumed to be large, $\mathscr{C}$ depends only on the dimensionless roughness z_r and standard formulae for steady currents can be used to estimate $\mathscr{C}$. The value of $\mathscr{C}$ turns out to range between 20 and 30. Furthermore, the function $F(\xi)$ ($\xi=(z^*-\eta^*)/(h^*+\eta^*)$) describes the vertical structure of the eddy viscosity. Following Dean (1974), $F(\xi)$ has been chosen such that the eddy viscosity grows linearly with the distance from the bed, when a region close to the bottom is considered, and then decreases achieving a finite small value at the free surface. Moreover, ν_{T0}^* is set equal to $kU_0^*h_0^*\int_{-1}^{0}F(\xi)\,\mathrm{d}\xi/\mathscr{C}$ and $\nu_T(\xi)=F(\xi)/\int_{-1}^{0}F(\xi)\,\mathrm{d}\xi$. It can be verified that the eddy viscosity ν_{T0}^* is $O(10^{-1})\,\mathrm{m^2\,s^{-1}}$. These definitions of ν_{T0}^*

and ν_T have been chosen in such a way that the depth-averaged value of $\nu_T(\xi)$ is equal to one. Since ν_{T0}^* is proportional to U_0^*, it is useful to introduce the new viscous parameter

$$\hat{\Delta} = \frac{k\int_{-1}^{0} F(\xi)\,\mathrm{d}\xi}{\mathscr{C}} = \frac{\hat{\delta}^2}{\hat{r}}, \tag{2.31}$$

which does not depend on the strength of the tidal current. Finally, note that using a time-independent model for ν_T^* might be considered a severe approximation. However, as pointed out by Gerkema (2000), it provides a fair description of the phenomenon since it mainly fails only at flow reversal when tidal currents are very weak and the transport of any quantity, and in particular of sediment, tends to vanish.

Once the flow is determined by solving (2.25)–(2.28), the evaluation of the bottom shear stress closes the problem.

3. The time development of arbitrary bottom perturbations of small amplitude

Small perturbations of the flat bottom are considered so that the bottom configuration differs from the flat one by a small (strictly infinitesimal) amount proportional to ϵ ($\epsilon \ll 1$). Hence, the bottom profile can be thought to be given by the superposition of different spatial components which evolve independently from each other. A normal mode analysis can be performed and the problem can be solved for the generic spatial component such that the dimensionless water depth is given by

$$h = 1 - \epsilon A(t)\mathrm{e}^{\mathrm{i}(\alpha_x x+\alpha_y y)} + c.c. + O(\epsilon^2), \tag{3.1}$$

where $\epsilon A(t)$ is the amplitude of the generic component which is periodic in the x and y directions with dimensionless wavenumbers α_x and α_y. The small value of ϵ allows for the hydrodynamic variables to be expanded in terms of ϵ

$$\begin{aligned}(u, v, w, p, \eta) = &\left(u_0, v_0, \frac{h_0^*}{L^*}w_0, \frac{L^*}{h_0^*}p_0, \frac{a^*}{h_0^*}e_0\right)\\ &+\epsilon\left(u_1, v_1, w_1, \hat{r}\,p_1, \left(\frac{a^*}{h_0^*}\right)^2 e_1\right)A(t)\mathrm{e}^{\mathrm{i}(\alpha_x x+\alpha_y y)} + c.c. + O(\epsilon^2),\end{aligned} \tag{3.2}$$

where $a^* = U_0^* h_0^*/(\omega^* L^*)$ and $L^* = \sqrt{g^* h_0^*}/\omega^*$ are the order of magnitude of the amplitude and the length of the tidal wave, respectively. Because of the use of a linear approach, all the perturbations of both the hydrodynamic variables (see (3.2)) and morphodynamic variables (see (3.3)–(3.5)) are sinusoidal functions of the x and y coordinates. Therefore, the knowledge of the complex amplitudes allows the evaluation of the perturbations at any location along the bottom profile.

The hydrodynamic problems which are obtained at $\mathrm{O}(\epsilon^0)$ and $\mathrm{O}(\epsilon)$ by plugging (3.1) and (3.2) into (2.25)–(2.28) do not differ from those found by Blondeaux & Vittori (2005*a*, *b*) and the interested reader is referred to the above papers for a detailed description of the solution procedure.

Once the hydrodynamics is known, the perturbations of the bottom shear stresses and those of the sediment transport rates per unit fraction can be readily evaluated,

$$(\theta_{x,n}, \theta_{y,n}) = (\theta_{x,n,0}, \theta_{y,n,0}) + \epsilon A(t)(\theta_{x,n,1}, \theta_{y,n,1})\mathrm{e}^{\mathrm{i}(\alpha_x x+\alpha_y y)} + c.c. + O(\epsilon^2), \tag{3.3}$$

$$\left(Q_{x,n}^{(u)}, Q_{y,n}^{(u)}\right) = \left(Q_{x,n,0}^{(u)}, Q_{y,n,0}^{(u)}\right) + \epsilon A(t)\left(Q_{x,n,1}^{(u)}, Q_{y,n,1}^{(u)}\right)\mathrm{e}^{\mathrm{i}(\alpha_x x+\alpha_y y)} + c.c. + O(\epsilon^2). \tag{3.4}$$

Since the algebra, though straightforward, is lengthy and tedious, we omit the details.

Because $\epsilon \ll 1$, it is possible to expand the volume fractions of the sediment classes in the form

$$(p_{a,n}, p_{i,n}, p_{s,n}) = (p_{a,n,0}, p_{i,n,0}, p_{s,n,0}) + \epsilon A(t)(p_{a,n,1}, p_{i,n,1}, p_{s,n,1})\mathrm{e}^{\mathrm{i}(\alpha_x x+\alpha_y y)} + c.c. + O(\epsilon^2). \quad (3.5)$$

Because of the small value of L_a^*, the exchange of sediment between the substrate and the active layer makes the grain size distribution to deviate rapidly from the initial one and the linear approximation to hold only for very small bottom perturbations. In other words, the present analysis can describe only the very initial stages of the sand wave growth.

By substitution of (3.4) and (3.5) into (2.23), the contribution of each grain size class to the bed evolution at order ϵ becomes

$$p_{i,n,0}\frac{\mathrm{d}A}{\mathrm{d}t} + L_a\left(\frac{\mathrm{d}p_{a,n,1}}{\mathrm{d}t}A + p_{a,n,1}\frac{\mathrm{d}A}{\mathrm{d}t}\right) = -\beta\left[\mathrm{i}\alpha_x\left(p_{a,n,0}Q^{(u)}_{x,n,1} + p_{a,n,1}Q^{(u)}_{x,n,0}\right) + \mathrm{i}\alpha_y\left(p_{a,n,0}Q^{(u)}_{y,n,1} + p_{a,n,1}Q^{(u)}_{y,n,0}\right)\right]A. \quad (3.6)$$

Note that the sediment transport of each grain size class at order ϵ consists of a contribution that is related to the flow over a wavy bottom and a contribution that is induced by the changes in the sea bottom composition. Moreover, since $L_a^* = z_r^*$ and the ripple height is assumed to be constant, the dimensionless thickness L_a of the active layer is constant.

To determine the solution, it is necessary to specify the initial conditions, i.e. the initial stratigraphy of the sea bottom. Let us consider an initial uniform distribution of the sediment classes such that

$$p_{i,n,0} = p_{a,n,0} = p_{s,n,0} = p_{n,0}, \quad (3.7)$$

the value of $p_{n,0}$ being constant both in space and time. The problem can be further simplified taking into account that the dimensionless quantity $L_a = L_a^*/h_0^*$ and the parameter β are of the same order of magnitude and both are much smaller than one. Hence, (3.6) reduces to

$$L_a\frac{\mathrm{d}p_{n,1}}{\mathrm{d}t}A + \frac{\mathrm{d}A}{\mathrm{d}t}p_{n,0} = -\beta\left[\mathrm{i}\alpha_x\left(p_{n,0}Q^{(u)}_{x,n,1} + p_{n,1}Q^{(u)}_{x,n,0}\right) + \mathrm{i}\alpha_y\left(p_{n,0}Q^{(u)}_{y,n,1} + p_{n,1}Q^{(u)}_{y,n,0}\right)\right]A \quad (3.8)$$

where $p_{a,n,1}$ is written as $p_{n,1}$ to simplify the notation. Indeed, $L_a p_{n,1}$ can be neglected with respect to $p_{n,0}$ since $p_{n,1}$ are assumed to be of the same order as $p_{n,0}$. In Appendix A the effects of the neglected term on the time development of $p_{n,1}$ are determined and it is shown that the results described in the following are practically coincident with those obtained taking into account the term $L_a p_{n,1}$, as long as the phenomenon is analysed for a number of tidal cycles of order 10^3. Moreover, in Appendix A it is shown that the effects of the term $L_a p_{n,1}$ become significant only when $p_{n,1}$ becomes large. This happens only when the number of tidal cycles is larger than $O(10^3)$, such that a linear analysis cannot be used anymore to describe the time development of the bottom perturbation since its amplitude has attained significant values.

Integrating (3.8) over all the grain sizes and taking into account the constraints $\sum_{n=1}^{N} p_{n,0} = 1$, $\sum_{n=1}^{N} p_{n,1} = 0$, it follows

$$\frac{\mathrm{d}A}{\mathrm{d}t} = -\beta \sum_{n=1}^{N} \left[\mathrm{i}\alpha_x \left(p_{n,0} Q^{(u)}_{x,n,1} + p_{n,1} Q^{(u)}_{x,n,0} \right) + \mathrm{i}\alpha_y \left(p_{n,0} Q^{(u)}_{y,n,1} + p_{n,1} Q^{(u)}_{y,n,0} \right) \right] A. \tag{3.9}$$

By using (3.9), equation (3.8) becomes

$$\begin{aligned} L_a \frac{\mathrm{d}p_{n,1}}{\mathrm{d}t} - p_{n,0}\beta \sum_{m=1}^{N} \left[\mathrm{i}\alpha_x \left(p_{m,0} Q^{(u)}_{x,m,1} + p_{m,1} Q^{(u)}_{x,m,0} \right) + \mathrm{i}\alpha_y \left(p_{m,0} Q^{(u)}_{y,m,1} + p_{m,1} Q^{(u)}_{y,m,0} \right) \right] \\ = -\beta \left[\mathrm{i}\alpha_x \left(p_{n,0} Q^{(u)}_{x,n,1} + p_{n,1} Q^{(u)}_{x,n,0} \right) + \mathrm{i}\alpha_y \left(p_{n,0} Q^{(u)}_{y,n,1} + p_{n,1} Q^{(u)}_{y,n,0} \right) \right], \end{aligned} \tag{3.10}$$

from which $p_{n,1}$ can be determined. The reader should notice that, since the critical value of the Shields parameter depends on the mean grain size (see (2.14)), the functions $Q^{(u)}_{x,n,1}$ and $Q^{(u)}_{y,n,1}$ depend on $p_{n,1}$. This dependence should be made explicit using (2.3) in order to solve (3.9), (3.10) and to determine $p_{n,1}$. In other words, it is necessary to write

$$\left(Q^{(u)}_{x,n,1}, Q^{(u)}_{y,n,1} \right) = \left(\hat{Q}^{(u)}_{x,n,1}, \hat{Q}^{(u)}_{y,n,1} \right) + \left(\hat{\hat{Q}}^{(u)}_{x,n,1}, \hat{\hat{Q}}^{(u)}_{y,n,1} \right) \sum_{m=1}^{N} \frac{d^*_m}{d^*_{mean,0}} p_{m,1}. \tag{3.11}$$

Once $p_{n,1}$ are evaluated, (3.9) provides the time development of the amplitude of the bottom perturbation.

In the following, to keep the solution procedure and the analysis of the results as simple as possible, we fix $N = 2$ and consequently, $d^*_1 = d^*_{mean,0}(1-\sigma)$, $d^*_2 = d^*_{mean,0}(1+\sigma)$. It follows that the perturbation of the grain size distribution is known when the value of $p_{1,1} = -p_{2,1}$ is determined.

By using (3.11), we obtain

$$\frac{\mathrm{d}p_{1,1}}{\mathrm{d}t} + p_{1,1} \frac{\beta}{L_a} \left[-p_{1,0} \mathscr{F}(t) + \mathscr{H}(t) \right] = p_{1,0} \frac{\beta}{L_a} \left[\mathscr{G}(t) - \mathscr{I}(t) \right], \tag{3.12}$$

where $\mathscr{F}(t)$, $\mathscr{G}(t)$, $\mathscr{H}(t)$ and $\mathscr{I}(t)$ are periodic functions with frequency ω^* whose expressions are given in Appendix B. The solution of (3.12) can be found by writing

$$p_{1,1}(t) = \mathrm{e}^{-\int_0^t \frac{\beta}{L_a} \left[-p_{1,0} \mathscr{F}(t') + \mathscr{H}(t') \right] \mathrm{d}t'} \mathscr{K}(t), \tag{3.13}$$

it follows:

$$\frac{\mathrm{d}\mathscr{K}}{\mathrm{d}t} = \frac{\beta}{L_a} \frac{p_{1,0} \left[\mathscr{G}(t) - \mathscr{I}(t) \right]}{\mathrm{e}^{-\int_0^t \frac{\beta}{L_a} \left[-p_{1,0} \mathscr{F}(t') + \mathscr{H}(t') \right] \mathrm{d}t'}}. \tag{3.14}$$

Since the right-hand side of (3.14) turns out to be a periodic function of time, we expand it as a Fourier series of time. Then the solution can be written in the form

$$\mathscr{K} = \sum_{n=-\infty, n\neq 0}^{\infty} \mathscr{K}_n \mathrm{e}^{\mathrm{i}nt} + \mathscr{K}_0 t + C_1, \tag{3.15}$$

where the values of $\mathscr{K}_n$ can be obtained once the harmonic components of the right-hand side of (3.14) are evaluated. Hence, the function $p_{1,1}$ turns out to be

$$p_{1,1}(t) = \mathrm{e}^{-\int_0^t \frac{\beta}{L_a} \left[-p_{1,0} \mathscr{F}(t') + \mathscr{H}(t') \right] \mathrm{d}t'} \left(\sum_{n=-\infty, n\neq 0}^{\infty} \mathscr{K}_n \mathrm{e}^{\mathrm{i}nt} + \mathscr{K}_0 t + C_1 \right), \tag{3.16}$$

where the constant C_1 depends on the initial conditions, i.e. on the initial value $p_{1,1}(0)$ of $p_{1,1}(t)$

$$C_1 = p_{1,1}(0) - \sum_{n=-\infty, n\neq 0}^{\infty} \mathscr{K}_n. \tag{3.17}$$

Then, the temporal growth of the amplitude of the bottom forms can be determined by means of (3.9) which gives rise to the following amplitude equation

$$\frac{1}{A}\frac{\mathrm{d}A}{\mathrm{d}t} = -\beta \left\{ \mathscr{D}(t)\mathscr{F}(t) \left(\sum_{n=-\infty, n\neq 0}^{\infty} \mathscr{K}_n \mathrm{e}^{\mathrm{i}nt} + \mathscr{K}_0 t + C_1 \right) + \mathscr{G}(t) \right\}, \tag{3.18}$$

where the function $\mathscr{D}(t)$, defined by

$$\mathscr{D}(t) = \mathrm{e}^{-\int_0^t \frac{\beta}{L_a}\left[-p_{1,0}\mathscr{F}(t')+\mathscr{H}(t')\right]\mathrm{d}t'} = \sum_{n=-\infty}^{\infty} \mathscr{D}_n \mathrm{e}^{\mathrm{i}nt}, \tag{3.19}$$

turns out to be a periodic function of time. If we note that the function,

$$\Gamma(t) = -\mathscr{D}(t)\mathscr{F}(t) \left(\sum_{n=-\infty, n\neq 0}^{\infty} \mathscr{K}_n \mathrm{e}^{\mathrm{i}nt} \right) - \mathscr{G}(t), \tag{3.20}$$

is also a periodic function of time with a non-vanishing time average value $\overline{\Gamma}$ ($\Gamma(t) = \overline{\Gamma} + \tilde{\Gamma}(t)$) and we write

$$\mathscr{L}(t) = -\mathscr{D}(t)\mathscr{F}(t) = \sum_{n=-\infty, n\neq 0}^{\infty} \mathscr{L}_n \mathrm{e}^{\mathrm{i}nt} + \mathscr{L}_0, \tag{3.21}$$

it follows that

$$A(t) = A_0 \exp\left(\beta \left[\int_0^t \tilde{\Gamma}\mathrm{d}t + \sum_{n=-\infty, n\neq 0}^{\infty} \frac{\mathscr{L}_n}{n} \left(\frac{\mathscr{K}_0}{n} - \mathrm{i}C_1 \right) \mathrm{e}^{\mathrm{i}nt} \right] \right)$$
$$\exp\left(\beta \left[\sum_{n=-\infty, n\neq 0}^{\infty} \frac{\mathscr{L}_n}{\mathrm{i}n} t \mathrm{e}^{\mathrm{i}nt} \right] \right) \exp(\beta[\overline{\Gamma}t + C_1\mathscr{L}_0 t]). \tag{3.22}$$

In (3.22) use has been made of the vanishing of the product $\mathscr{K}_0\mathscr{L}_0$. The first exponential term on the right-hand side of (3.22) describes the periodic oscillations of the bottom forms which take place during the tidal cycle and are characterized by a constant amplitude. The second exponential term describes oscillations which grow in time. In both cases the oscillations are small because they are proportional to the small quantity β. The last exponential term on the right-hand side describes the growth/decay of the bottom forms which takes place because of the inherent instability of the morphodynamic system. As indicated in the previous section, the growth takes place on the slow morphodynamic time scale $T = \beta t$ and it is controlled by the value of $\overline{\Gamma}$ and by the product $C_1\mathscr{L}_0$. The growth described by the term $\exp(C_1\mathscr{L}_0 T)$ depends on the initial perturbation of the grain size distribution and the value of $C_1\mathscr{L}_0$ can be made positive or negative or equal to zero with an appropriate choice of $p_{1,1}(0)$. Physically, it means that the growth/decay of the bottom perturbation, which is controlled by the value of $\overline{\Gamma}$, can be accelerated or decelerated depending on the initial grain size perturbation. In other words, the process which leads to the formation of sand waves, when the sea bed is made of a sediment mixture, can be

accelerated or decelerated if a perturbation of the grain size distribution is added to the bottom perturbation. However, since the value of $\mathscr{L}_0$ turns out to be much smaller than $\overline{\Gamma}$, the initial grain size distribution has small effects on the growth of the bottom perturbation unless $p_{1,1}(0)$ has quite large unrealistic values. Moreover, since both the amplitude and the phase of the initial perturbation of the grain size distribution are arbitrary, in the following the stability/instability of the sea bed configuration is chosen to be discussed by considering the value of $\overline{\Gamma}$ only and the effects of $p_{1,1}(0)$ on the phenomenon are not taken into account.

The aim of the analysis is twofold. On one hand, we want to evaluate the effects that a grain size mixture has on the process which leads to the formation of sand waves. On the other hand, we want to investigate the sorting process induced by the bed form growth. The grain size distribution can be analysed looking at the value of $p_{1,1}$

$$p_{1,1}(t) = \mathscr{D}(t)\left(\sum_{n=-\infty,n\neq 0}^{\infty} \mathscr{K}_n \mathrm{e}^{\mathrm{i}nt} + \mathscr{K}_0 t + C_1\right). \tag{3.23}$$

Taking into account (3.19), we can write

$$\begin{aligned} p_{1,1}(t) = &\sum_{n=-\infty,n\neq 0}^{\infty} \mathscr{D}_n \mathrm{e}^{\mathrm{i}nt} \sum_{n=-\infty,n\neq 0}^{\infty} \mathscr{K}_n \mathrm{e}^{\mathrm{i}nt} + \mathscr{D}_0 \sum_{n=-\infty,n\neq 0}^{\infty} \mathscr{K}_n \mathrm{e}^{\mathrm{i}nt} \\ &+ \mathscr{K}_0 t \sum_{n=-\infty,n\neq 0}^{\infty} \mathscr{D}_n \mathrm{e}^{\mathrm{i}nt} + \mathscr{K}_0 \mathscr{D}_0 t + C_1 \sum_{n=-\infty,n\neq 0}^{\infty} \mathscr{D}_n \mathrm{e}^{\mathrm{i}nt} + C_1 \mathscr{D}_0, \end{aligned} \tag{3.24}$$

where different contributions can be recognized. The last two terms are due to the initial value of the grain size perturbation which causes both oscillations and a mean value different from zero. The second and third term represent oscillations of the grain size distribution induced by the periodic nature of the tidal flow. Therefore, the grain size distribution averaged over the tidal cycle, is controlled by the time-averaged value of the first term of the right-hand side of (3.24) and by the value of the product $\mathscr{K}_0\mathscr{D}_0$. Of course, for large times the latter term prevails on the former such that the resulting mean grain size distribution on the morphodynamic time scale is controlled by the value of $\mathscr{K}_0\mathscr{D}_0$. The values of $p_{1,1}(t)$ obtained by means of (3.24) and by the numerical integration of (A 1) are compared with $\mathscr{K}_0\mathscr{D}_0 t$ in Appendix A. The obtained results (see figure 17) show that the value of $\mathscr{K}_0\mathscr{D}_0 t$ fully describes the net growth/decay of $p_{1,1}$ even though only the full solution can describe the oscillations of the grain size distribution taking place during the tide cycle. Moreover, it appears that the effect of the initial value of $p_{1,1}$ becomes negligible as the time grows. If no initial perturbation is given to $p_{1,1}$, the results of Appendix A (see figure 18) show that the value of $\mathscr{K}_0\mathscr{D}_0 t$ can describe the grain size distribution for a large number of cycles until the growth of the amplitude of the bottom forms makes the linear approach unsuitable to describe the phenomenon. Hence, in the discussion of the results, only the value of $\mathscr{K}_0\mathscr{D}_0$ as function of the parameters of the problem is analysed in detail. Appendix A clarifies this points more thoroughly.

4. Discussion of the results

4.1. *Description of the results*

Because of the large number of the parameters controlling the phenomenon, an exhaustive description of the results in the parameter space is not possible. Hence,

in the following, we simply compare the results of the present analysis with those obtained for a uniform sediment with a diameter equal to the mean diameter of the mixture, considering tide and sediment characteristics which are typical of shallow tidal seas. The comparison allows us to understand the qualitative and quantitative effects that a mixture has on the process which leads to the formation of sand waves. The reader interested into the effects that the other parameters of the problem have on the phenomenon is referred to Besio *et al.* (2006).

The results presented in the following show that the effects of a sediment mixture on the formation of sand waves are somewhat weak and perhaps smaller than those that other phenomena presently neglected (e.g. the spring-neap tide cycle) might have. Rather than evaluating the quantitative results provided by the analysis, the reader should consider the qualitative findings, e.g. the stabilizing/destabilazing effect that a mixture has on the flat bottom configuration or the trend of the coarse fraction of the sediment mixture to be piled up at the crests/troughs of the bottom forms.

We consider parameter values typical for the North Sea (van der Veen 2008). The average water depth is 30 m and the dominant tide constituent is assumed to be the M2 component with a maximum value of the depth-averaged velocity equal to $0.70\,\mathrm{m\,s^{-1}}$. Moreover, e is 0.2 and the tidal velocity vector is counter-clockwise rotating. Finally, the sediment has a value of $d^*_{mean,0}$ equal to 0.4 mm and the bottom roughness is assumed to be due to sea ripples which are 0.22 m long and 2.2 cm high (Soulsby & Whitehouse 2005). For these values of the parameters, the ratio between the shear velocity and the fall velocity turns out to be smaller than one. Therefore, the assumption of a negligible contribution of the suspended load to the sediment transport appears feasible. The dimensionless parameters of the model turn out to be $\hat{r} = 166$, $\hat{\Delta} = 2.61\ 10^{-3}$, $e = 0.2$, $z_r = 0.837\ 10^{-3}$, $d_{mean,0} = 1.33\ 10^{-5}$, $\Psi_{mean} = 2.74\ 10^{-3}$ and $R_{p,mean} = 23.7$. Since the field data considered by Roos *et al.* (2007*a*) show that values of $\sigma = \sigma^*/d^*_{mean,0}$ fall between 0.1 for well-sorted mixtures to 0.3 for poorly sorted mixtures, the theoretical results have been obtained for values of σ ranging between 0 (homogeneous sediment) and 0.5 (poorly sorted sand mixtures).

Since Besio *et al.* (2006) showed that the most amplified modes are those characterized by crests orthogonal to the main axis of the tidal ellipse, we focus our attention on this case. Therefore, we introduce the axes $(\hat{x}, \hat{y})$ such that $\hat{x}$ is aligned with the main axis of the tidal ellipse and we consider perturbations characterized by $\alpha_{\hat{y}}$ equal to zero. Moreover, because of the symmetry of the forcing flow, no migration of the bottom forms is expected to be present and indeed the results show that the imaginary part $\overline{\Gamma}_I$ of $\overline{\Gamma}$ vanishes.

Figure 2 shows the amplification rate $\overline{\Gamma}_R$ of the bottom perturbation versus its wavenumber $\alpha_{\hat{x}}$ for both a perfectly sorted sediment and a mixture characterized by a dimensionless standard deviation σ equal to 0.3. In this case, the theoretical predictions show that the flat bottom configuration is more stable when the sea bed is made up of a poorly sorted sediment than when the sediment is well sorted. In fact, the dimensional response time T^*_Γ turns out to be about 9200 days for a uniform sediment and 9600 days for a graded sediment. Moreover, the results show that the bed forms which appear when the sea bed is made up of a mixture are longer than those which characterize a uniform sea bed. More specifically, the wavelengths for which the maximum amplification rate is attained are about 500 m and 540 m for the uniform sediment and the sediment mixture, respectively. The tendency of a mixture to stabilize the flat bed and to give rise to longer bed forms with respect to those appearing for a well-sorted sediment is similar to the tendency found by Foti & Blondeaux (1995*a*, *b*), who investigated ripple formation under sea waves.

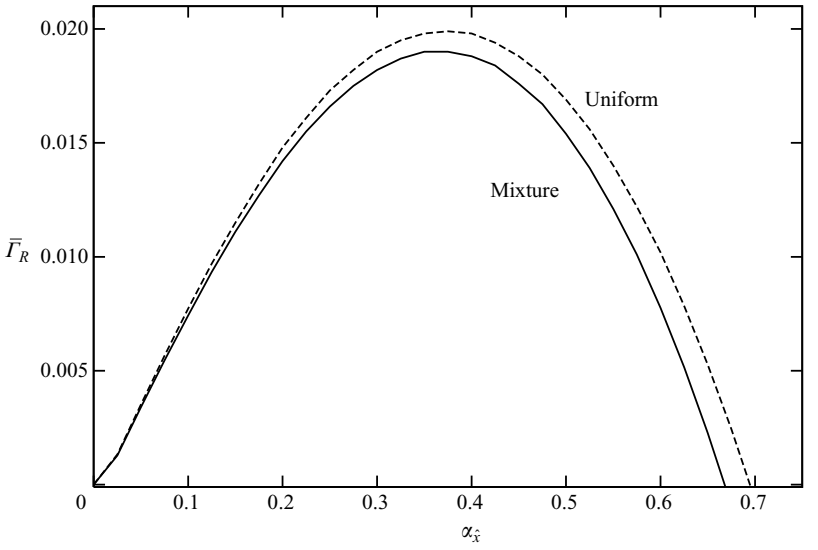

FIGURE 2. Amplification rate $\overline{\Gamma}_R$ of the bottom perturbation as function of $\alpha_{\hat{x}}$ for $\hat{r} = 166$, $\hat{\Delta} = 2.61\ 10^{-3}$, $e = 0.2$, $z_r = 0.837\ 10^{-3}$, $d_{mean,0} = 1.33\ 10^{-5}$, $\Psi_{mean} = 2.74\ 10^{-3}$ and $R_{p,mean} = 23.7$. The broken line corresponds to a uniform sediment and the continuous line is related to a graded sediment characterized by $\sigma = 0.3$.

To consider the spatial variation of the bed composition, we point out that the mean grain size can be written in the form

$$d^*_{mean} = d^*_{mean,0} + \epsilon \left[d^*_{mean,1} A(t) \mathrm{e}^{\mathrm{i}(\alpha_x x + \alpha_y y)} + c.c. \right] + O(\epsilon^2). \tag{4.1}$$

The real part of $d^*_{mean,1}$ describes variations of the mean grain size which are in or out of phase with respect to the elevation of the bottom profile while the imaginary part corresponds to a shift of the grain size distribution with respect to the bottom forms. For a bimodal sediment mixture ($N = 2$), (4.1) can be written as

$$\frac{d^*_{mean}}{d^*_{mean,0}} = 1 + \epsilon \left[A(t) p_{1,1} (d_1 - d_2) \mathrm{e}^{\mathrm{i}(\alpha_x x + \alpha_y y)} + c.c. \right] + O(\epsilon^2). \tag{4.2}$$

Since d_1 is chosen to be smaller than d_2, a positive value of the real part of $p_{1,1}$ implies an accumulation of the fine fraction at the crests of the bottom forms, while a negative value indicates a coarsening of the sediment at the crests. The imaginary part of $p_{1,1}$ quantifies the possible shift of the grain size distribution with respect to the bottom waviness. Since, for large times, the value of $p_{1,1}$ is dominated by the term $\mathscr{K}_0 \mathscr{D}_0$, which turns out to be real and negative, the results of figure 3 indicate that the coarse fraction tends to be piled up at the crests of the bottom forms.

Figure 4 shows the effect, on the phenomenon, of the sortedness of the sediment mixture. In figure 4, $\overline{\Gamma}_R$ is plotted versus $\alpha_{\hat{x}}$ both for a uniform well-sorted sediment and different bimodal mixtures characterized by the same mean diameter but different values of the dimensionless standard deviation σ. Of course when σ tends to vanish, the results of the uniform case are recovered. At first, when σ increases from zero up to about $\sigma = 0.3$, the growth rate of the bottom perturbations decreases. Then a further increase of σ leads to an increase of $\overline{\Gamma}_R$ and for σ equal to 0.4 and 0.5 the values of $\overline{\Gamma}_R$ become larger than those characterizing the uniform sediment and a sediment mixture destabilizes the flat bed configuration. Also the wavelength

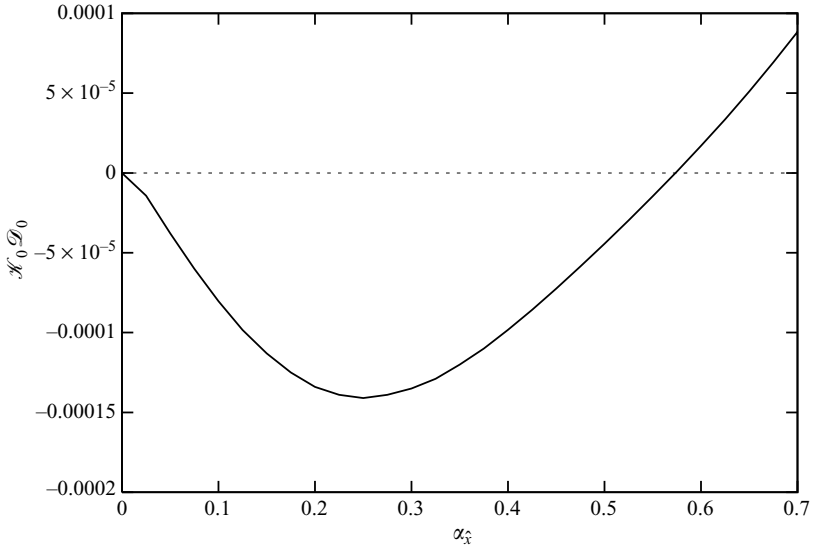

FIGURE 3. Values of $\mathscr{K}_0\mathscr{D}_0$ as function of $\alpha_{\hat{x}}$ for $\hat{r} = 166$, $\hat{\Delta} = 2.61\ 10^{-3}$, $e = 0.2$, $z_r = 0.837\ 10^{-3}$, $d_{mean,0} = 1.33\ 10^{-5}$, $\Psi_{mean} = 2.74\ 10^{-3}$ and $R_{p,mean} = 23.7$. The graded sediment is characterized by $\sigma = \sigma^*/d^*_{mean,0} = 0.3$.

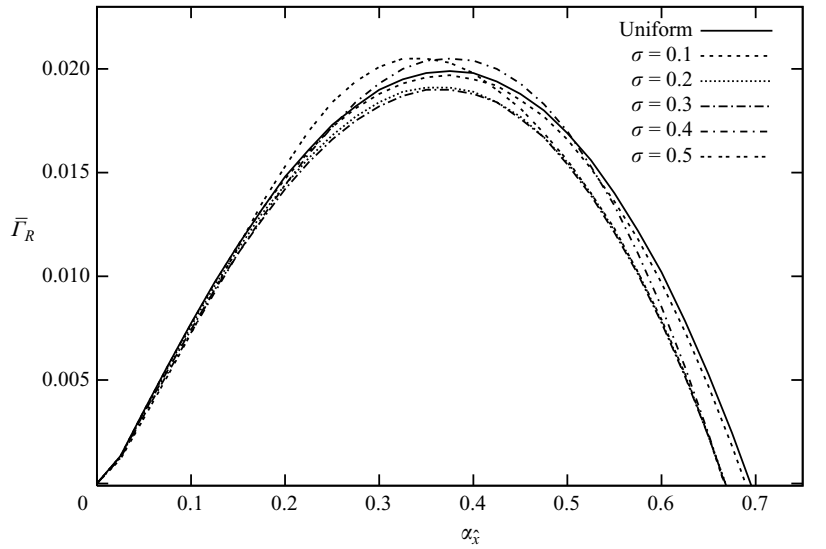

FIGURE 4. Amplification rate $\overline{\Gamma}_R$ of the bottom perturbation as function of $\alpha_{\hat{x}}$ for $\hat{r} = 166$, $\hat{\Delta} = 2.61\ 10^{-3}$, $e = 0.2$, $z_r = 0.837\ 10^{-3}$, $d_{mean,0} = 1.33\ 10^{-5}$, $\Psi_{mean} = 2.74\ 10^{-3}$ and $R_{p,mean} = 23.7$. The continuous line corresponds to a uniform sediment and the broken lines are related to a graded sediment characterized by different values of σ.

of the most unstable modes appears to depend on σ. For moderate values of σ the wavelength of the predicted bottom forms tends to be longer than that of a uniform sediment. However, as σ is increased, the wavelength first decreases and then increases and eventually becomes larger than the wavelength characterizing the well-sorted sediment.

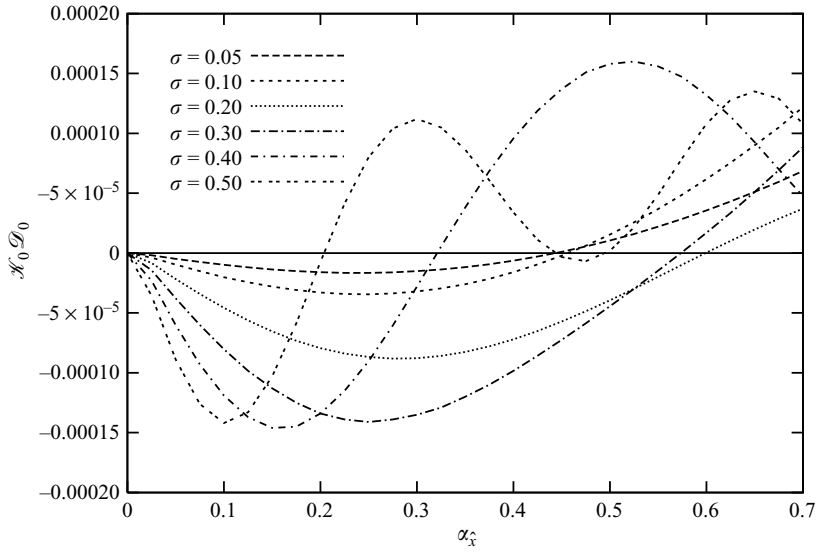

FIGURE 5. Values of $\mathscr{K}_0\mathscr{D}_0$ as function of $\alpha_{\hat{x}}$ for $\hat{r} = 166$, $\hat{\Delta} = 2.61\ 10^{-3}$, $e = 0.2$, $z_r = 0.837\ 10^{-3}$, $d_{mean,0} = 1.33\ 10^{-5}$, $\Psi_{mean} = 2.74\ 10^{-3}$, $R_{p,mean} = 23.7$ and different values of σ.

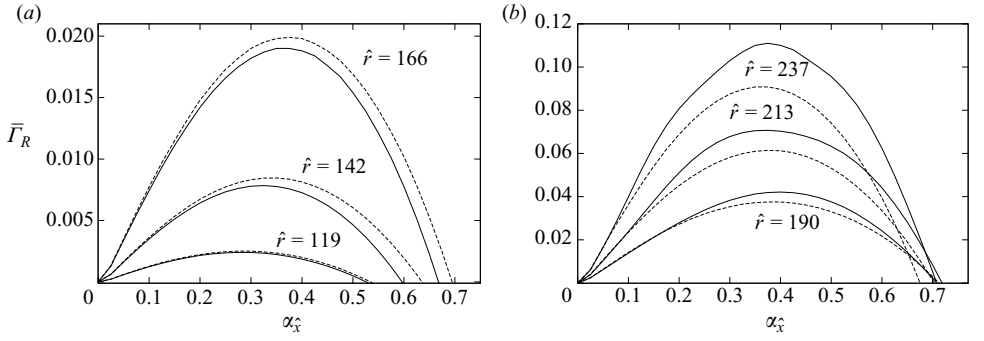

FIGURE 6. Amplification rate $\overline{\Gamma}_R$ of the bottom perturbation as function of $\alpha_{\hat{x}}$ for (*a*) $\hat{r} = 119$, 142, 166 and (*b*) $\hat{r} = 190$, 213, 237. The other parameter values are $\hat{\Delta} = 2.61\ 10^{-3}$, $e = 0.2$, $z_r = 0.837\ 10^{-3}$, $d_{mean,0} = 1.33\ 10^{-5}$, $\Psi_{mean} = 2.74\ 10^{-3}$ and $R_{p,mean} = 23.7$. The broken lines correspond to a uniform sediment and the continuous lines are related to a graded sediment characterized by $\sigma = 0.3$.

The influence of σ on the sorting process is illustrated in figure 5, where $\mathscr{K}_0\mathscr{D}_0$ is plotted versus $\alpha_{\hat{x}}$ for the same values of the parameters as those of figure 4. The results show that the sediment becomes coarser at the crest for well-sorted and moderately sorted sediment mixtures. However, for poorly sorted mixtures, the value of $\mathscr{K}_0\mathscr{D}_0$ becomes positive for the most preferred wavelength and a fining of the sediment takes place at the crests of the bottom forms.

Figure 6 shows the growth rate $\overline{\Gamma}_R$ of the bottom perturbations for different values of $\hat{r}$, considering a uniform sediment and a moderately sorted sediment ($\sigma = 0.3$). For moderate values of $\hat{r}$, i.e. for relatively weak tidal currents just larger than the critical value for which the sediment moves and sand waves appear, the growth rate which characterizes the graded sediment is always smaller than that obtained for a uniform

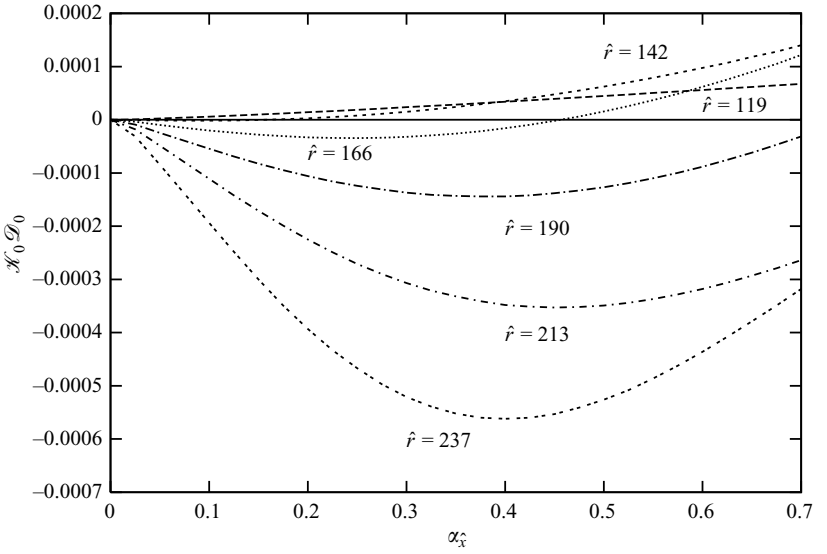

FIGURE 7. Values of $\mathscr{K}_0\mathscr{D}_0$ as function of $\alpha_{\hat{x}}$ for $\hat{r} = 119, 142, 166, 190, 213, 237$, $\hat{\Delta} = 2.61\ 10^{-3}$, $e = 0.2$, $z_r = 0.837\ 10^{-3}$, $d_{mean,0} = 1.33\ 10^{-5}$, $\Psi_{mean} = 2.74\ 10^{-3}$, $R_{p,mean} = 23.7$ and a graded sediment characterized by $\sigma = 0.1$.

sediment, thus showing that a graded sediment characterized by $\sigma = 0.3$ stabilizes the flat bed configuration. On the other hand, if strong tidal currents are considered, it is found that the presence of a mixture destabilizes the flat bed configuration (see figure 6*b*). The value of $\hat{r}$ at which the transition between stabilizing/destabilizing effects takes place, depends on the parameters of the problem and in particular on the value of σ. More specifically, for the values considered in figure 6 the threshold value of $\hat{r}$ is about 180 but, in the investigated range of the parameters, when σ is increased the threshold value of $\hat{r}$ decreases.

Figure 7 quantifies the sorting process which takes place when the bottom forms start to appear, considering bimodal mixtures characterized by a value of σ equal to 0.1 and different values of $\hat{r}$. It is found that for moderate values of the Keulegan–Carpenter number the value of $\mathscr{K}_0\mathscr{D}_0$ is positive indicating a fining of the crest. However, increasing the strength of the tide, the value of $\mathscr{K}_0\mathscr{D}_0$ becomes negative for the fastest growing wavenumber such that an accumulation of the coarse grains on the crests of the bed forms occurs. In figure 8, the same results as in figure 7 are reported but considering a less well sorted bimodal mixture ($\sigma = 0.3$). For moderate and intermediate values of the Keulegan–Carpenter number ($\hat{r} = 119$, 142, 166) the sorting process is similar to the results previously described, i.e. for moderate values of $\hat{r}$ a fining of the crest occurs and an increase of $\hat{r}$ leads to a coarsening at the crest. However, figure 8 reveals that poorly sorted sediment mixtures introduce a dependence of the value of $\mathscr{K}_0\mathscr{D}_0$ on $\alpha_{\hat{x}}$ when strong tidal currents are considered, such that both a coarsening as well as a fining of the crest can take place depending on the value of $\hat{r}$.

The results plotted in figures 6–8 have been obtained for fixed values of σ. The results of additional experiments, in which the influence of σ on the growth rate and the sorting process were investigated, are summarized in figures 9–12. Figures 9 and 10 show $\overline{\Gamma}_R$ versus $\alpha_{\hat{x}}$ for the same values of the parameters as those of figure 4 but for a smaller ($\hat{r} = 119$) and a larger ($\hat{r} = 213$) value of $\hat{r}$. In both cases, only a poorly

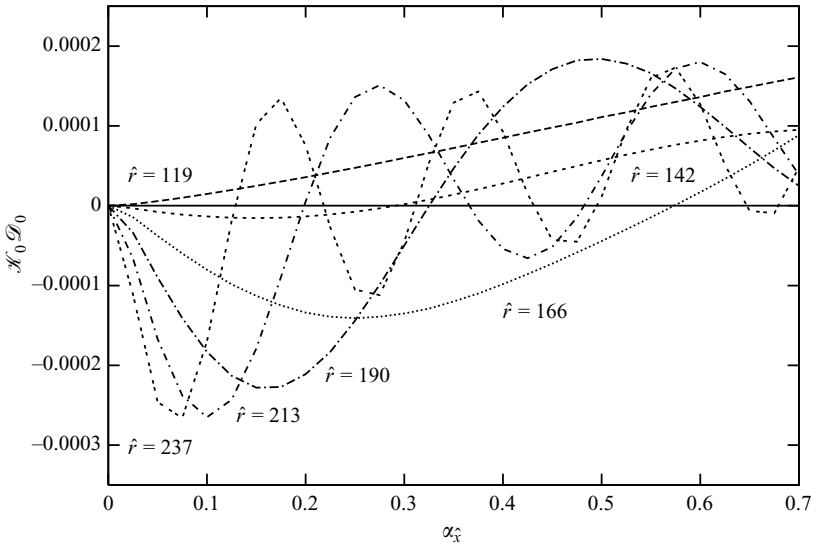

FIGURE 8. Values of $\mathscr{K}_0\mathscr{D}_0$ as function of $\alpha_{\hat{x}}$ for $\hat{r} = 119, 142, 166, 190, 213, 237$, $\hat{\Delta} = 2.61\ 10^{-3}$, $e = 0.2$, $z_r = 0.837\ 10^{-3}$, $d_{mean,0} = 1.33\ 10^{-5}$, $\Psi_{mean} = 2.74\ 10^{-3}$, $R_{p,mean} = 23.7$ and a graded sediment characterized by $\sigma = 0.3$.

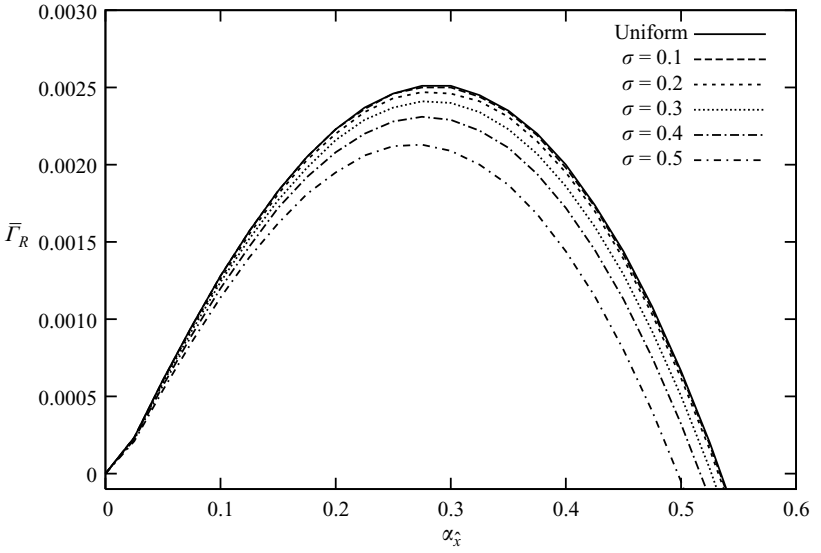

FIGURE 9. Amplification rate $\overline{\Gamma}_R$ of the bottom perturbation as function of $\alpha_{\hat{x}}$ for $\hat{r} = 119$, $\hat{\Delta} = 2.61\ 10^{-3}$, $e = 0.2$, $z_r = 0.837\ 10^{-3}$, $d_{mean,0} = 1.33\ 10^{-5}$, $\Psi_{mean} = 2.74\ 10^{-3}$ and $R_{p,mean} = 23.7$. The continuous line corresponds to a uniform sediment and the broken lines are related to graded sediment characterized by different values of σ.

sorted sediment shows large differences with respect to the uniform case. For the weakest tidal current, the mixture tends to stabilize the flat bed configuration and the wavelength of the most preferred mode is longer. On the other hand, for the strongest tidal current, a sediment mixture characterized by significant values of σ tends to destabilize the flat bed and both larger and smaller wavelengths with respect to a

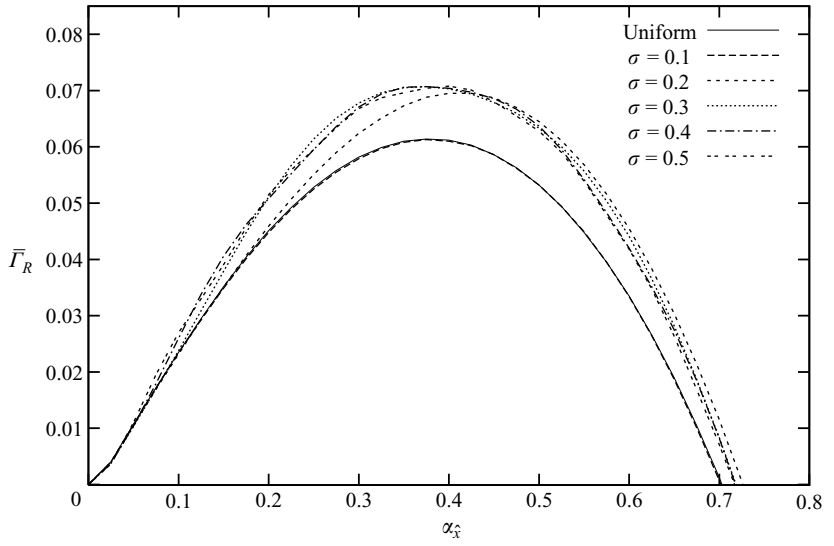

FIGURE 10. Amplification rate $\overline{\Gamma}_R$ of the bottom perturbation as function of $\alpha_{\hat{x}}$ for $\hat{r} = 213$, $\hat{\Delta} = 2.61\ 10^{-3}$, $e = 0.2$, $z_r = 0.837\ 10^{-3}$, $d_{mean,0} = 1.33\ 10^{-5}$, $\Psi_{mean} = 2.74\ 10^{-3}$ and $R_{p,mean} = 23.7$. The continuous line corresponds to a uniform sediment and the broken lines are related to graded sediment characterized by different values of σ.

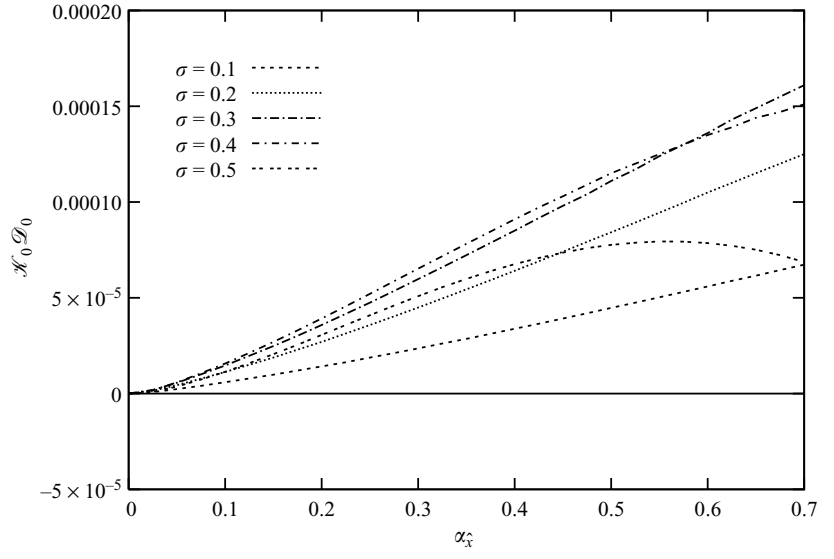

FIGURE 11. Values of $\mathscr{K}_0\mathscr{D}_0$ as function of $\alpha_{\hat{x}}$ for $\hat{r} = 119$, $\hat{\Delta} = 2.61\ 10^{-3}$, $e = 0.2$, $z_r = 0.837\ 10^{-3}$, $d_{mean,0} = 1.33\ 10^{-5}$, $\Psi_{mean} = 2.74\ 10^{-3}$, $R_{p,mean} = 23.7$ and different values of σ.

uniform sediment are predicted (see figure 10). The results plotted in figure 11 show that, for $\hat{r} = 119$, the fine fraction tends to pile up at the crests of the growing bottom perturbations independently of the value of σ. However, for $\hat{r} = 213$, as also observed in figures 5 and 8, for well-sorted sediment mixtures the grain size distribution is found coarser at the crest and for more poorly sorted mixtures the value of $\mathscr{K}_0\mathscr{D}_0$

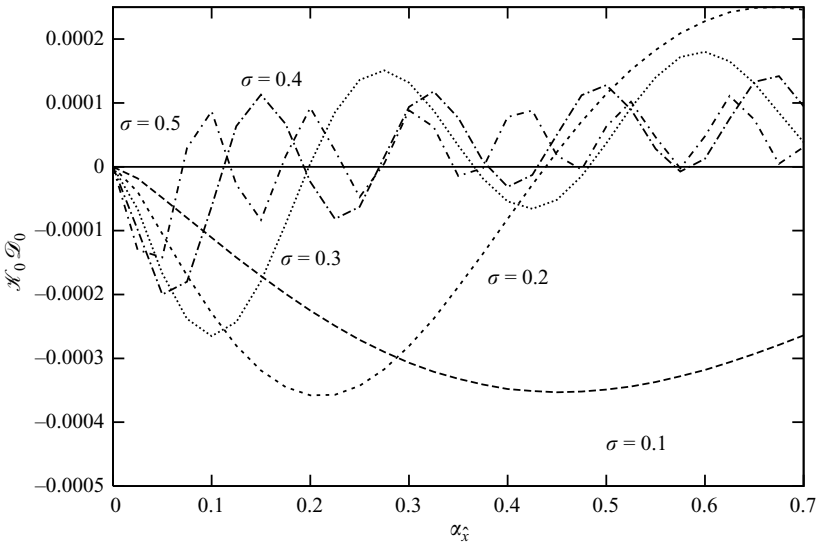

FIGURE 12. Values of $\mathscr{K}_0\mathscr{D}_0$ as function of $\alpha_{\hat{x}}$ for $\hat{r} = 213$, $\hat{\Delta} = 2.61\ 10^{-3}$, $e = 0.2$, $z_r = 0.837\ 10^{-3}$, $d_{mean,0} = 1.33\ 10^{-5}$, $\Psi_{mean} = 2.74\ 10^{-3}$, $R_{p,mean} = 23.7$ and different values of σ.

oscillates between negative and positive values increasing $\alpha_{\hat{x}}$ such that the sorting process is very sensitive to the value of σ (see figure 12).

4.2. *Physical interpretation and discussion*

To explain the predicted grain size distribution along the bed forms, it is necessary to consider different contributions. Indeed, the value of $\overline{d_{mean,1}}$ depends on the value of $\overline{p_{1,1}}$ which in turn depends on the sediment transport rate. Since the motion of the sediment, both at the leading order of approximation and at order ϵ, is induced by the complex interaction among fluid drag, gravitational force and sheltering effects, the understanding of the mechanism controlling the grain sorting is not straightforward. However, the obtained results can be understood taking into account a combination of two mechanisms. The first is related to the balance of the hiding/exposure effect and its effect on the mobility, and the second to differences in the number of recirculating cells felt by the distinct grain size classes.

For well-sorted sediment mixtures, the first mechanism gives rise to a shift from a fining to a coarsening of the bottom material at the crests of the bottom forms when the value of $\hat{r}$ is increased. Indeed, considering well-sorted mixtures and elaborating on the different contributions to $\mathscr{K}_0\mathscr{D}_0$ yields that the sign of $\mathscr{K}_0\mathscr{D}_0$ is qualitatively controlled by the sign of the real part of $C(t) = (\beta/L_a)\,[\mathscr{G}(t) - \mathscr{I}(t)]$ averaged over the tidal cycle. Since the procedure that leads to the latter statement is lengthy, but straightforward, we omit the details. Taking into account that $p_{1,0} + p_{2,0}$ is equal to one, $\overline{C}$ can be written as

$$\overline{C} = p_{1,0}\alpha_{\hat{x}}\frac{\beta}{L_a}\left(\overline{\hat{Q}^{(u)}_{\hat{x},1,1}} - \overline{\hat{Q}^{(u)}_{\hat{x},2,1}}\right), \tag{4.3}$$

the imaginary part of which vanishes. The changes in the grain size distribution are related to the difference between the correction of net sediment transport rates of the fine and coarse fractions induced by the wavy bottom. As pointed out by Besio *et al.* (2006), the interaction of the oscillatory tidal current with the wavy bed generates a

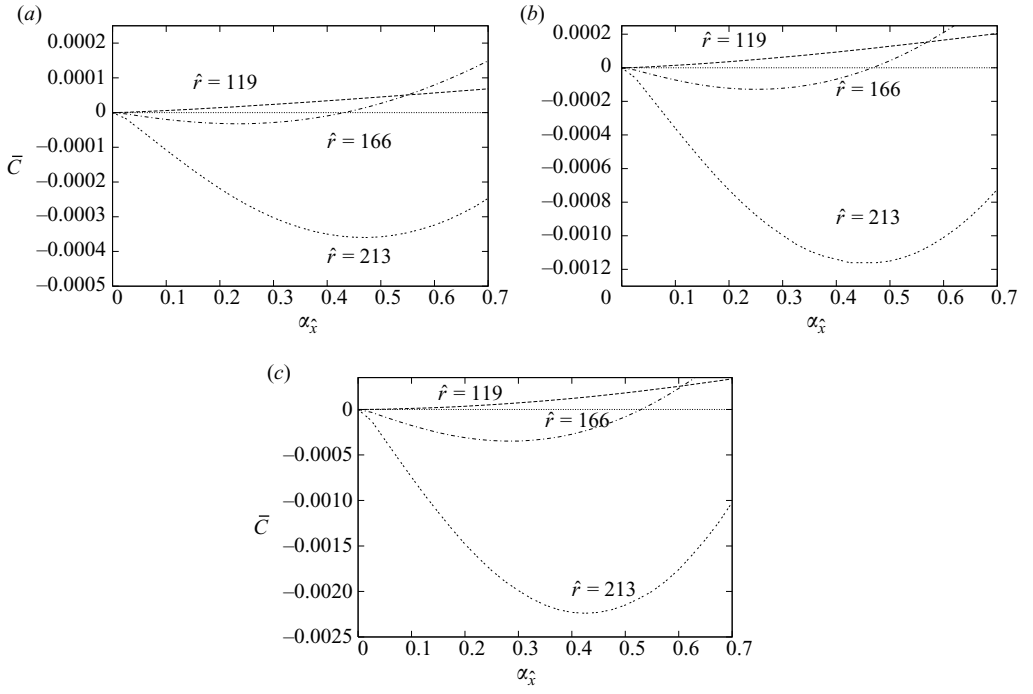

FIGURE 13. Values of $\overline{C}$ as function of $\alpha_{\hat{x}}$ for $\hat{r} = 119, 166$ and 213, $\hat{\Delta} = 2.61\ 10^{-3}$, $e = 0.2$, $z_r = 0.837\ 10^{-3}$, $d_{mean,0} = 1.33\ 10^{-5}$, $\Psi_{mean} = 2.74\ 10^{-3}$ and $R_{p,mean} = 23.7$. The sediment mixtures are characterized by (*a*) $\sigma = 0.1$, (*b*) $\sigma = 0.3$ and (*c*) $\sigma = 0.5$.

complex flow field which exhibits also steady velocity components in the form of two recirculating cells for each bottom form. The generation of a steady streaming due to the interaction of a spatially varying oscillatory flow with a rigid wall was first discovered in acoustics and theoretically analysed by Rayleigh (1884). Extension to sea waves was made by Longuet-Higgins (1953). A steady component is also generated by a uniform oscillatory flow interacting with a complex geometry (Stuart 1966; Lyne 1971). The interested reader can find a discussion of the physical mechanism originating a steady velocity component in the above mentioned papers. Taking into account (3.11), the reader should notice that $\hat{Q}^{(u)}_{\hat{x},n,1}$ represents the contribution to the sediment transport rate of order ϵ, which is induced by these steady recirculating cells. Figure 13(*a*) shows $\overline{C}$ as a function of $\alpha_{\hat{x}}$ for a moderate, intermediate and large value of the Keulegan–Carpenter number considering a well-sorted mixture ($\sigma = 0.1$). For weak tidal currents $\overline{C}$ is positive whereas, for strong tidal currents, $\overline{C}$ is negative. Hence, for moderate values of $\hat{r}$, the time average over a tidal cycle of $\hat{Q}^{(u)}_{\hat{x},1,1}$ is larger than that of $\hat{Q}^{(u)}_{\hat{x},2,1}$ and a fining of the sediment at the crest occurs. For strong tidal currents the contribution to the sediment transport of order ϵ related to the flow over a wavy bottom for the finer fraction is smaller than that of the coarser fraction, yielding a coarsening of the sediment at the crest. Physically, it means that, for weak tidal currents, the exposure effects cannot compensate for the reduced mobility of the coarse fraction of the sediment mixture. Therefore, the fine fraction is more easily transported towards the crests of the bottom perturbation by the steady recirculating cells generated by the interaction of the tidal current with the bottom waviness. For moderate and strong tidal currents, hiding effects increase and become dominant,

slowing down the transport of the fine fraction of the mixture. Hence, the steady velocity component associated to the recirculating cells has a larger effect on the coarse grains which are thus piled up at the crests of the bottom perturbation.

To understand the oscillations in the value of $\mathscr{K}_0\mathscr{D}_0$ which occur for poorly sorted mixtures and strong tidal currents, it is necessary to take into account a second mechanism. Indeed, as shown in figures 13(b) and 13(c), the mechanism just described is still present also for large values of $\hat{r}$ and poorly sorted mixtures ($\sigma = 0.3$ and $\sigma = 0.5$). However, on top of this mechanism, a second mechanism takes place which induces the oscillations in the value of $\mathscr{K}_0\mathscr{D}_0$. First, it is necessary to note that the velocity of the sediment particles is proportional to the shear velocity through a coefficient which depends on the grain size and decreases when the grain size is increased (Fredsøe & Deigaard 1992). Then, since the shear velocity is proportional to the depth-averaged velocity, the ratio s_s between the amplitude of the sediment displacement oscillations and the wavelength of the bottom forms, turns out to be proportional to the ratio s_f between the amplitude of the fluid displacement oscillations and the wavelength of the bottom forms. Finally, since s_f is proportional to $\alpha_{\hat{x}}\hat{r}$, it appears that s_s is also proportional to $\alpha_{\hat{x}}\hat{r}$. Hence, the value of s_s increases as $\alpha_{\hat{x}}\hat{r}$ is increased and, for large values of $\hat{r}$, the dynamics of the sediments is affected by a large number of steady recirculating cells which increases as $\alpha_{\hat{x}}$ is increased. Since s_s depends also on the grain size, the fine and coarse fractions of a sediment mixture feel the effects of a different number of steady recirculating cells and the net motion of the fine/coarse fraction can be towards the crests or the troughs depending on the values assumed by $\hat{r}$, $\alpha_{\hat{x}}$ and σ. For this reason the value of $\mathscr{K}_0\mathscr{D}_0$ alternates between negative and positive values as $\alpha_{\hat{x}}$ is increased and the frequency of the oscillations increases as $\hat{r}$ or σ are increased.

To analyse the behaviour of $\overline{\Gamma}_R$, we remind that $\Gamma(t)$ consists of two contributions described by (3.20). The second term on the right-hand side of (3.20), $\mathscr{G}(t)$, is the sum of the sediment transport rates of the fine and coarse grain size fractions induced by the bottom waviness while the first term on the right-hand side describes the influence on the amplification rate of the changes in the bottom composition. The reader can better understand the previous statement noting that $\mathscr{G}(t)$ is function of $\hat{Q}^{(u)}_{\hat{x},n,1}$ only and that the first term on the right-hand side of (3.20) is related to $p_{1,1}(t)$ (see equations (3.18)–(3.20)). In figures 14 and 15 the growth rate $\overline{\Gamma}_R$ and the contribution due to $-\overline{\mathscr{G}}_R$ are plotted as a function of $\alpha_{\hat{x}}$ considering a uniform sediment and sediment mixtures characterized by $\sigma = 0.3$ and 0.5 for weak and strong tidal currents, respectively. It is found that for weak tidal currents $\overline{\Gamma}_R$ is smaller than $-\overline{\mathscr{G}}_R$ while $\overline{\Gamma}_R$ becomes larger than $-\overline{\mathscr{G}}_R$ for strong tidal currents. Moreover, the contribution of $-\overline{\mathscr{G}}_R$, i.e. the contribution related to the sediment transport induced by the bottom waviness, to the amplification rate is always stabilizing with respect to the uniform case. Additionally, figures 14 and 15 yield that $-\overline{\mathscr{G}}_R$ does not influence the wavelength of the fastest growing wavenumber. It follows that the sorting process induced by the incipient growth of the bottom forms reduces $\overline{\Gamma}_R$ for weak tidal currents and enhances the amplification rate when strong tidal currents are considered. Furthermore, it can be concluded that the differences in the most preferred wavelength are induced by the influence of the sorting process on the growth of the bottom forms.

As already pointed out, the number of model parameters is so large that an exhaustive investigation of the results in the parameter space cannot be made. Further runs have shown that different values of the tide and sea characteristics (h_0^*, ϕ_0, e) as well as different values of the mean characteristics of the sediment ($d^*_{mean,0}$) do

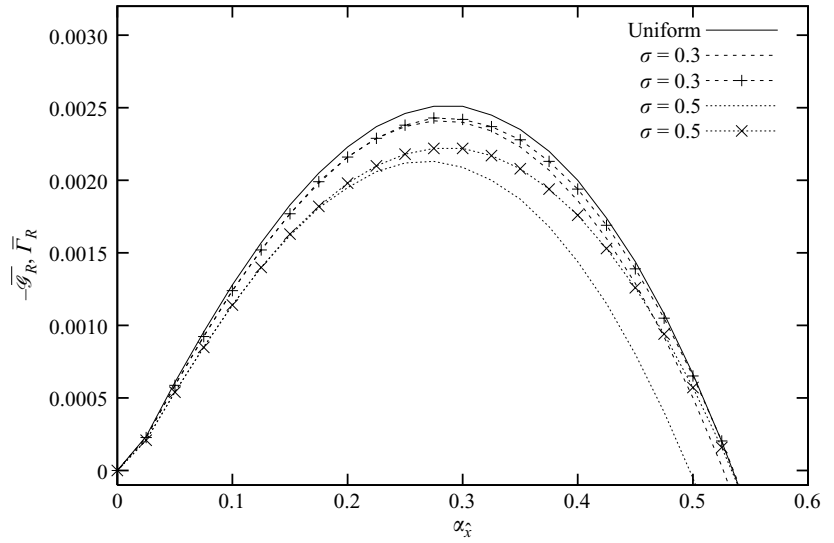

FIGURE 14. The amplification rate $\overline{\Gamma}_R$ and $-\overline{\mathscr{G}}_R$ as function of $\alpha_{\hat{x}}$ for $\hat{r} = 119$, $\hat{\Delta} = 2.61\ 10^{-3}$, $e = 0.2$, $z_r = 0.837\ \ 10^{-3}$, $d_{mean,0} = 1.33\ \ 10^{-5}$, $\Psi_{mean} = 2.74\ \ 10^{-3}$ and $R_{p,mean} = 23.7$. The continuous line corresponds to a uniform sediment, the broken lines to the amplification rate $\overline{\Gamma}_R$ and the lines with symbols to the value of $-\overline{\mathscr{G}}_R$. The sediment mixtures considered are characterized by a standard deviation equal to 0.3 and 0.5.

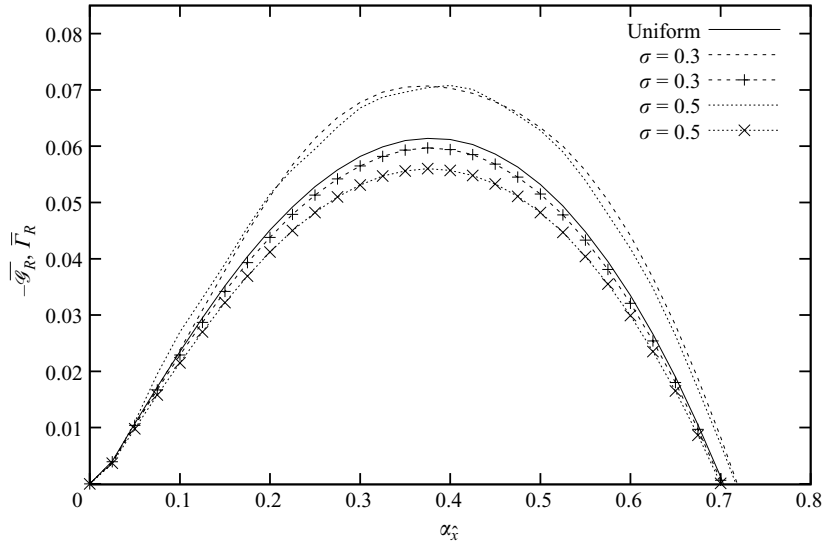

FIGURE 15. The amplification rate $\overline{\Gamma}_R$ and $-\overline{\mathscr{G}}_R$ as function of $\alpha_{\hat{x}}$ for $\hat{r} = 213$, $\hat{\Delta} = 2.61\ 10^{-3}$, $e = 0.2$, $z_r = 0.837\ \ 10^{-3}$, $d_{mean,0} = 1.33\ \ 10^{-5}$, $\Psi_{mean} = 2.74\ \ 10^{-3}$ and $R_{p,mean} = 23.7$. The continuous line corresponds to a uniform sediment, the broken lines to the amplification rate $\overline{\Gamma}_R$ and the lines with symbols to the value of $-\overline{\mathscr{G}}_R$. The sediment mixtures considered are characterized by a standard deviation equal to 0.3 and 0.5.

not imply qualitative changes on the sorting process previously described and results similar to those described so far have been obtained also for the amplification rate. However, it is found that when the mean grain size is decreased, the influence of the sorting process on the growth rate decreases such that, when a small mean grain size

is considered, only stabilizing effects of the mixture are observed and the wavelength remains practically unchanged.

At last, it is noted that to ascertain the sensitivity of the result to the sediment transport predictor, predictions of sand wave appearance have been made using other sediment transport rate formulae. Since the time required by the bed load to adapt to new flow conditions is much smaller than the tide period, any sediment transport rate formula, which provides reliable predictions of the sediment flux for steady flows, can be used. Presently, we have also employed the formula of Meyer-Peter & Muller (1948), corrected for slope effects (see also Fredsøe & Deigaard 1992). For the sake of space, these results are not reported herein. However, the obtained results qualitatively confirm the major findings previously described even though, unavoidably, quantitative differences (smaller than or in the order of 100 %) are present.

5. Comparison of theoretical predictions with field data

In the following we describe the outputs of a comparison between present results and field observations. Unfortunately, a detailed quantitative comparison cannot be made because of the paucity of field observations. The only data which are available to the authors are those described by Roos *et al.* (2007*a*), Van Lancker & Jacobs (2000) and Terwindt (1971). Roos *et al.* (2007*a*) describe the observations carried out at five sites in the continental shelf of the Netherlands, where sand waves are present (see figure 16). The grain size characteristics were measured at the crests of sand waves, at their troughs and in most cases also along the slopes of the bottom forms. At the site, named site 3 by Roos *et al.* (2007*a*), only two measurements were made (one at the crest and one at the trough of a bottom form) and the mean grain size at the crest is practically coincident with that at the trough. On the contrary, at the other sites (namely site 1, site 2, site 4 and site 5), a large number of sediment samples were taken and the mean grain size is the result of an average over a significant number of data. Moreover, the mean grain size at the crests differs appreciably from that at the troughs. It turns out that the grain size at the crests of the sand waves is larger than at the troughs at sites 1, 2, 4 while the opposite is observed at site 5. Van Lanker & Jacobs (2000) analysed the grain size distribution along the sand waves observed in the Western Belgian continental shelf and in particular near the Baland Bank situated offshore of Westende (see location 6 in figure 16). They found that the grain size is coarser at the crests than in the troughs. In Terwindt (1971), the observations at four locations North of the Hinder Banks in the Southern bight of the North Sea are described (see figure 16). The first location (location 7) is approximately at 50 km offshore the Dutch coast in front of the Eastern Scheldt. The second and third locations (locations 8 and 9) are very close to each other and are situated about 25 km offshore Hoek van Holland. The fourth location (location 10) is about 40 km offshore of Zandvoort. At all the sites, sand waves are present and a normal sieve analysis of grain size samples taken along these large-scale bottom forms reveals a grain size sorting pattern. At the first location, the field data show a fining of the grain size towards the crests of the sand waves. At the second and third locations the trend is reversed and the grain size increases when moving from the troughs towards the crests of the sand waves. At the fourth location no clear trend was recognized in the grain size distribution.

An analysis of the field data concerning the tidal current, the water depth and the sediment characteristics does not seem to justify the differences between the grain size distribution at sites 1, 2, 4, 6, 8, 9 and that at sites 5, 7. Indeed the data on the tidal

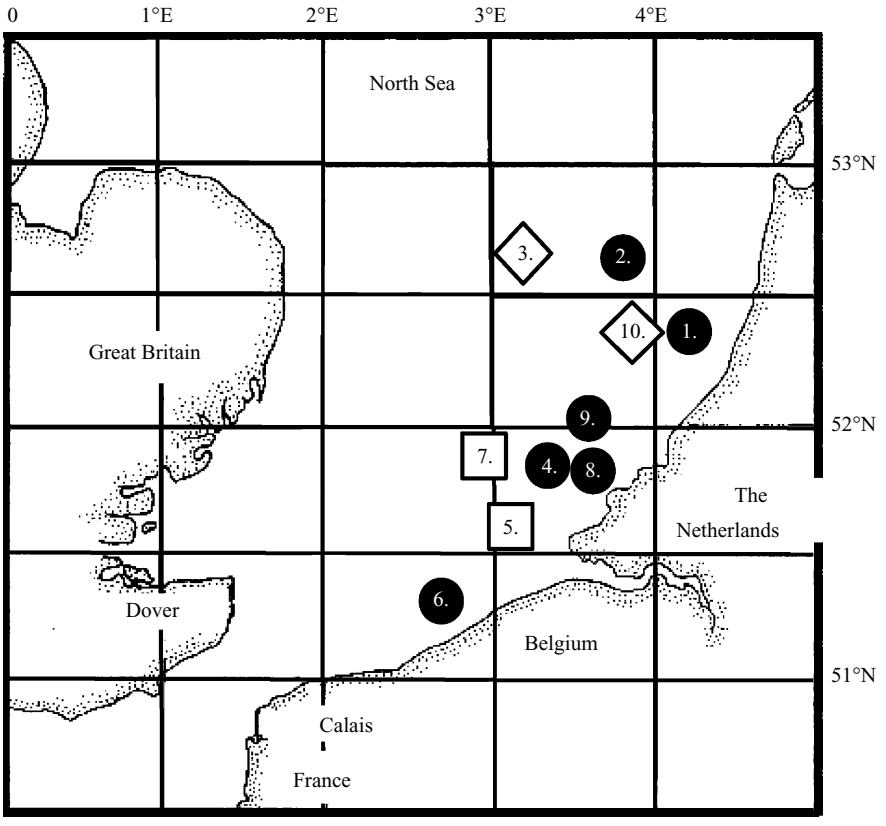

FIGURE 16. Sketch of the locations in the North Sea where field measurements of the grain size composition of the bottom material were carried out. At the locations indicated by a darkened circle, the coarse grains are observed at the crests of the sand waves. At the locations indicated by a box (locations 5 and 7), a fining of the sediment at the crests of the sand waves is observed. No clear trend is observed at locations 3 and 10 (indicated by a diamond).

velocity (van der Veen 2008) as well as those on the water depth (Boon & Gerritsen 1997; Ten Brummelhuis, Gerritsen & Van der Kaay 1997) and the median grain size (Rijks Geologische Dienst 1984; Hydrographer of the Navy 1992) do not show any clear correlation between the local conditions and the local grain size distribution.

A comparison of the theoretical results with field data is not rigorously justified, since the former are obtained by means of a linear analysis and the latter are affected, to some extent, by nonlinear effects. Notwithstanding this fact, the theoretical analysis seems to provide a possible explanation of the apparently conflicting field observations. Indeed, the findings of the theoretical model show that a coarsening of the sediment at the crests is as possible as a fining, depending on relatively small changes of the tidal current and of the sediment properties.

A more quantitative comparison between the theoretical predictions and the field data would be necessary to fully support the predictive capabilities of the present analysis and to verify that nonlinear effects play a minor role in the morphodynamic development of the bottom forms and on the grain size distribution. Since, to achieve this goal, detailed information on the oscillating forcing flow and on the bottom material is needed, laboratory experiments or very accurate field measurements should be specifically designed.

6. Conclusions

In this paper, a model is developed to study the initial formation of sand waves in shallow tidal seas characterized by a bottom that consists of a sediment mixture. The main goal of the work was the investigation of the sorting process induced by the incipient growth of sand waves and the evaluation of the effects that a graded sediment has on the formation of the bottom forms. To this aim we have compared the present results with those of Besio *et al.* (2006), who considered the uniform sediment case.

The analysis shows that both the formation of the bottom forms and the corresponding sorting process are sensitive to the value of the standard deviation σ of the bottom material and to the strength of the tidal current. More specifically, it is found that for moderate values of $\hat{r}$, i.e. for weak tidal currents, the graded sediment tends to stabilize the flat bottom configuration and to give rise to longer wavelengths. Moreover, the fine fraction of the mixture piles up at the crests of the bottom forms while the coarse fraction moves towards the troughs. On the other hand, for large values of $\hat{r}$, a graded sediment destabilizes the flat bottom configuration with respect to the uniform sediment case and both longer and shorter wavelengths can be found depending on σ. Moreover, for large values of $\hat{r}$, the sediment at the crest becomes coarser than that at the trough for well-sorted mixtures. Considering increasing values of σ, both a coarsening and a fining at the crest can occur depending on the value of σ. Note that, for large values of $\hat{r}$, it would be necessary to include the evaluation of the suspended load to have a more accurate description of the phenomenon (Blondeaux & Vittori 2009). The change from a fining to a coarsening of the crests, which is found for well-sorted mixtures when $\hat{r}$ is increased, is related to a changing balance between hiding/exposure effects and reduced mobility effects. For moderate values of $\hat{r}$, the reduced mobility of the larger grains dominates on hiding/exposure effects and an accumulation of the finer grains at the crests takes place. For strong tidal currents, the hiding/exposure effects prevail and the larger grains are found to move towards the crests of the bottom forms. The dependence of the sorting process on the value of σ for strong tidal currents is found to be related to the different number of wave crests that the coarse and fine fractions cross during a tide cycle. This implies that the coarse and fine fractions feel the effects of a different number of steady recirculating cells and this difference changes as the tidal strength or σ are changed.

The present findings provide a possible explanation of the apparently conflicting field observations described in Roos *et al.* (2007*a*), Van Lancker & Jacobs (2000) and Terwindt (1971). The presence, at some locations, of the coarse fraction at the crests of the sand waves while the opposite occurs at other locations could be related to minor differences in the local tidal current and bottom material. However, in the field also nonlinear effects e.g. vertical sorting and the shape of the sand wave, play a role in the resulting sediment distribution. Therefore, the comparison of the model results with the field observations cannot be considered conclusive.

This research has been supported by the Ministero dell'Universitá e della Ricerca. Initial stage funding was also provided by the University of Genova. The youngest author wishes to acknowledge the E. U. for a grant in the framework of the FLUBIO project. Both authors are grateful to Professor H. E. de Swart for valuable discussions and comments on an earlier draft of the manuscript. One anonymous reviewer is thanked for constructive comments and suggestions which have helped to improve the manuscript considerably.

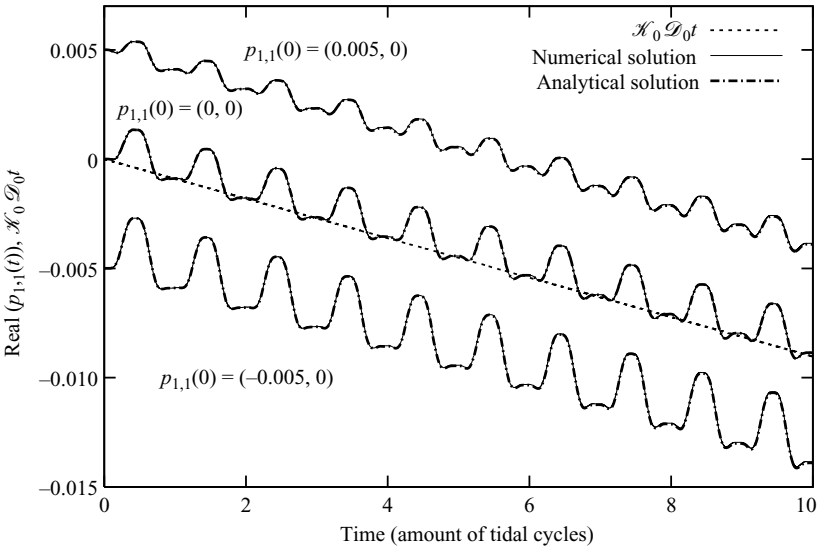

FIGURE 17. The values of the real part of $p_{1,1}(t)$ and $\mathscr{K}_0\mathscr{D}_0 t$ for the fastest growing wavenumber ($\alpha_{\hat{x}} = 0.375$) plotted versus time during 10 tidal cycles for $\hat{r} = 190$, $\hat{\Delta} = 2.61\ 10^{-3}$, $e = 0.2$, $z_r = 0.837\ 10^{-3}$, $d_{mean,0} = 1.33\ 10^{-5}$, $\Psi_{mean} = 2.74\ 10^{-3}$ and $R_{p,mean} = 23.7$. The graded sediment is characterized by $\sigma = 0.1$. The continuous lines correspond to the numerical solution of (A 1) and the broken lines are the analytical solution (3.16). Different initial values of $p_{1,1}(t)$ are considered. From the bottom to the top: $p_{1,1}(0) = (-0.005, 0)$, $(0, 0)$ and $(0.005,0)$.

Appendix A

The results described in § 4 have been obtained neglecting the term $L_a p_{n,1}$ in (3.8). Without this simplification, equation (3.12), which describes the time development of $p_{1,1}(t)$, would be

$$\frac{\mathrm{d}\ p_{1,1}}{\mathrm{d}t} + p_{1,1}\frac{\beta}{L_a}[-p_{1,0}\mathscr{F}(t) + \mathscr{H}(t)] = p_{1,0}\frac{\beta}{L_a}[\mathscr{G}(t) - \mathscr{I}(t)] + \beta\left[\mathscr{G}(t)p_{1,1} + \mathscr{F}(t)p_{1,1}^2\right]. \tag{A 1}$$

Equation (A 1) can be solved numerically employing a standard Runge–Kutta method of the second order. In the following, we compare the analytical solution of (3.12) presented in § 3 with the numerical solution of (A 1). Figure 17 shows the real part of $p_{1,1}$, plotted versus time, during 10 tidal cycles considering different initial values of $p_{1,1}(t)$ for the fastest growing wavenumber ($\alpha_{\hat{x}} = 0.375$). The Keulegan–Carpenter number is equal to 190, σ is set equal to 0.1 and the other parameters are equal to those considered in figure 2. The solution of the nonlinear equation (A 1) and the analytical solution are practically coincident, confirming that the term $L_a p_{n,1}(t)$ is negligible considering a small number of tidal cycles. Additionally, figure 17 shows that the initial value of $p_{1,1}(t)$ does not qualitatively influence the sorting process for large times. Moreover, it is found that the coefficient $\mathscr{K}_0\mathscr{D}_0$, which is chosen to represent the sorting process, captures the qualitative characteristics of the resulting grain size distribution.

Figure 18 illustrates the characteristics of the time development of the real part of $p_{1,1}(t)$ described by (A 1) and the value of $\mathscr{K}_0\mathscr{D}_0 t$ for very large times, considering the same input parameters as in figure 17 and $p_{1,1}(0) = (0, 0)$. The reader should notice that in figure 18 the oscillations of $p_{1,1}$ taking place during the tidal cycle are

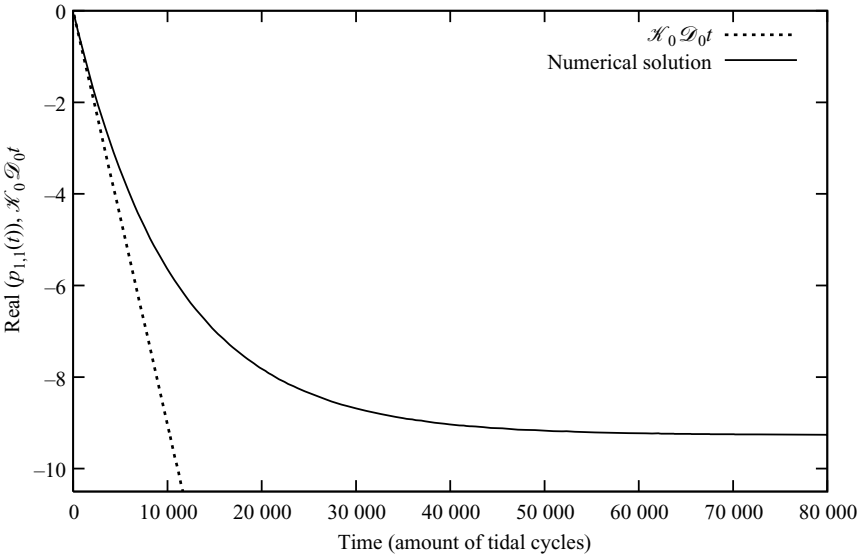

FIGURE 18. The values of the real part of $p_{1,1}(t)$ and $\mathscr{K}_0\mathscr{D}_0 t$ for the fastest growing wavenumber ($\alpha_{\hat{x}} = 0.375$) plotted versus time for $\hat{r} = 190$, $\hat{\Delta} = 2.61\ 10^{-3}$, $e = 0.2$, $z_r = 0.837\ 10^{-3}$, $d_{mean,0} = 1.33\ 10^{-5}$, $\Psi_{mean} = 2.74\ 10^{-3}$ and $R_{p,mean} = 23.7$. The graded sediment is characterized by $\sigma = 0.1$ and $p_{1,1}(0) = (0, 0)$ is considered. The continuous line corresponds to the numerical solution of (A 1) and the broken line is $\mathscr{K}_0\mathscr{D}_0 t$.

filtered out. The numerical integration of (A 1) shows that the value of $p_{1,1}$ reaches a periodic state after a long transient growth. This periodic state is attained when $p_{1,1}(t)$ is so large that $\beta[\mathscr{G}(t)p_{1,1} + \mathscr{F}(t)p_{1,1}^2]$ is no longer negligible with respect to the other terms appearing in (A 1). As shown in figure 18, this periodic state cannot be described by (3.12). However, $p_{1,1}(t)$ attains this periodic state only after such a large number of tidal cycles ($\sim$ 60 000 tidal cycles) that the amplitude of the bottom perturbations is expected to be large and a linear stability analysis to fail. Indeed, the dimensional response time T_r^* of the bed forms is of the order of 10 000 days ($\sim$ 20 000 tidal cycles). Hence, to predict sand wave appearance, it appears that the transient behaviour should be investigated and not the periodic state.

Appendix B

The periodic functions $\mathscr{F}(t)$, $\mathscr{G}(t)$, $\mathscr{H}(t)$ and $\mathscr{I}(t)$ are given by

$$\mathscr{F}(t) = \Bigg\{ \mathrm{i}\alpha_x \big(Q^{(u)}_{x,1,0} - Q^{(u)}_{x,2,0}\big) + \mathrm{i}\alpha_y \big(Q^{(u)}_{y,1,0} - Q^{(u)}_{y,2,0}\big) + (d_1 - d_2)\left[\mathrm{i}\alpha_x \left(p_{1,0}\hat{\hat{Q}}^{(u)}_{x,1,1} + p_{2,0}\hat{\hat{Q}}^{(u)}_{x,2,1}\right) + \mathrm{i}\alpha_y \left(p_{1,0}\hat{\hat{Q}}^{(u)}_{y,1,1} + p_{2,0}\hat{\hat{Q}}^{(u)}_{y,2,1}\right)\right]\Bigg\}, \quad \text{(B 1)}$$

$$\mathscr{G}(t) = \big[p_{1,0}\big(\mathrm{i}\alpha_x \hat{Q}^{(u)}_{x,1,1} + \mathrm{i}\alpha_y \hat{Q}^{(u)}_{y,1,1}\big) + p_{2,0}\big(\mathrm{i}\alpha_x \hat{Q}^{(u)}_{x,2,1} + \mathrm{i}\alpha_y \hat{Q}^{(u)}_{y,2,1}\big)\big], \quad \text{(B 2)}$$

$$\mathscr{H}(t) = \left[\mathrm{i}\alpha_x Q^{(u)}_{x,1,0} + \mathrm{i}\alpha_y Q^{(u)}_{y,1,0} + (d_1 - d_2)p_{1,0}\left(\mathrm{i}\alpha_x \hat{\hat{Q}}^{(u)}_{x,1,1} + \mathrm{i}\alpha_y \hat{\hat{Q}}^{(u)}_{y,1,1}\right)\right], \quad \text{(B 3)}$$

$$\mathscr{I}(t) = \big(\mathrm{i}\alpha_x \hat{Q}^{(u)}_{x,1,1} + \mathrm{i}\alpha_y \hat{Q}^{(u)}_{y,1,1}\big). \quad \text{(B 4)}$$

REFERENCES

Antia, E. E. 1996 Shoreface-connected ridges in German and US mid-Atlantic bights: similarities and contrasts. *J. Coast. Res.* **12**, 141–146.

Ashida, K. & Michiue, M. 1972 Study on hydraulic resistance and bedload transport rate in alluvial streams. *Japan Soc. Civ. Engng* **206**, 59–69.

van den Berg, J. & Van Damme, R. M. J. 2005 Sand wave simulation on large domains. In *Proc. RCEM'05* (ed. G. Parker & M. H. Garcia). Taylor & Francis/Balkema.

Besio, G., Blondeaux, P., Brocchini, M., Hulscher, S. J. M. H., Idier, D., Knaapen, M. A. P., Nemeth, A. A., Roos, P. C. & Vittori, G. 2008 The morphodynamics of tidal sand waves: a model overview. *Coast. Engng* **55** (7–8), 657–670.

Besio, G., Blondeaux, P. & Frisina, P. 2003 A note on tidally generated sand waves. *J. Fluid Mech.* **485**, 171–190.

Besio, G., Blondeaux, P. & Vittori, G. 2006 On the formation of sand waves and sand banks. *J. Fluid Mech.* **557**, 1–27

Blondeaux, P. & Vittori, G. 2005*a* Flow and sediment transport induced by tide propagation. Part 1. The flat bottom case. *J. Geophys. Res.* **110** (C7), C07020, doi:10.1029/2004JC002532.

Blondeaux, P. & Vittori, G. 2005*b* Flow and sediment transport induced by tide propagation. Part 2. The wavy bottom case. *J. Geophys. Res.* **110** (C8), C08003, doi:10.1029/2004JC002545.

Blondeaux, P. & Vittori, G. 2009 The formation of tidal sand waves: steady versus unsteady approaches. *J. Hydraulic Res.* **47** (2), 213–222.

Boon, J. G. & Gerritsen, H. 1997 Modelling of suspended particulate matter (SPM) in the North Sea: a detailed orthogonal boundary-fitted modelling approach (PROMISE). *Res Rep.* Z2025. Delft Hydraulics, Delft, The Netherlands.

Brownlie, W. R. 1981 Prediction of flow depth and sediment discharge in open channel. *Res Rep.* KH-R-43A. W. M. Keck Laboratory of Hydraulics and Water Resources, California Institute of Technology, Pasadena, CA.

Cherlet, J., Besio, G., Blondeaux, P., Van Lancker, V., Verfaillie, E. & Vittori, G. 2007 Modelling sand wave characteristics in Belgian continental shelf and in the Calais-Dover strait. *J. Geophys. Res.* **112**, C06002, doi:10.1029/2007JC004089.

Colombini, M. 2004 Revisiting the linear theory of sand dune formation. *J. Fluid Mech.* **502**, 1–16.

Dean, R. B. 1974 *AERO Report 74-11*. Imperial College, London.

Egiazaroff, I. V. 1965 Calculation of non-uniform sediment concentrations. *J. Hydraul. Engng* **91** (4), 225–248.

Foti, E. & Blondeaux, P. 1995*a* Sea ripple formation: the turbulent boundary layer case. *Coast. Engng* **25** (3–4), 227–236.

Foti, E. & Blondeaux, P. 1995*b* Sea ripple formation: the heterogenous sediment case. *Coast. Engng* **25** (3–4), 237–253.

Fredsøe, J. & Deigaard, R. 1992 Mechanics of coastal sediment transport. In *Advanced Series on Ocean Engineering*. World Scientific.

Gao, S., Collins, M. B., Lanckneus, J., De Moor, G. & Van Lancker, V. 1994 Grain-size trends associated with net sediment transport patterns: an example from the Belgian continental shelf. *Mar. Geol.* **121**, 171–185.

Gerkema, T. 2000 A linear stability analysis of tidally generated sand waves. *J. Fluid Mech.* **417**, 303–322.

Hirano, M. 1971 On river bed degradation with armoring. *Trans. Japan Soc. of Civil Eng.* **3** (2), 194–195.

Houthuys, R., Trentesaux, A. & De Wolf, P. 1994 Storm influences on a tidal sandbank's surface (Middelkerke Bank, southern North Sea). *Mar. Geol.* **121**, 23–41.

Hulscher, S. J. M. H. 1996 Tidal-induced large-scale regular bed form patterns in a three-dimensional shallow water model. *J. Geophys. Res.* **101** (C9), 20727–20744.

Hydrographer of the Navy. 1992 Spurn, East Anglia: associated British Ports, Thames estuary. Taunton, England, UK.

Kovacs, A. & Parker, G. 1994 A new vectorial bedload formulation and its application to the time evolution of straight river channels. *J. Fluid Mech.* **267**, 153–183.

Lanckneus, J., De Moor, G. & Stolk, A. 1994 Environmental setting, morphology and volumetric evolution of the Middelkerke Bank (southern North Sea). *Mar. Geol.* **121**, 1–21.

Longuet-Higgins, M. S. 1953 Mass transport in water waves. *Phil. Trans. R. Soc.* A. **345**, 535–581.

Lyne, W. H. 1971. Unsteady viscous flow over a wavy wall. *J. Fluid Mech.* **50**, 33–48.

Meyer-Peter, E. & Muller, R. 1948 Formulas for bed-load transport. In *Proceedings of the Second Congress I.A.H.R.*, Stockholm, pp. 39–64.

Parker, G. 2007 Transport of gravel and sediment mixtures. Private communication.

Passchier, S. & Kleinhans, M. G. 2005 Observations of sand waves, megaripples and hummocks in the Dutch coastal area and their relation to currents and combined flow conditions. *J. Geophys. Res.* **110**, F04S15, doi:10.1029/2004JF000215.

Rayleigh, L. 1884 On the circulation of air observed in Kundt's tubes, and on some allied acoustical problems. *Phil. Trans. R. Soc.* **175**, 1–21.

Rijks Geologische Dienst. 1984 *Geological Charts of the North Sea: Indefatigable, Flemish Bight, Ostend*. Haarlem.

Roos, P. C., Hulscher, S. J. M. H., van der Meer, F., van Dijk, T. A. G. P., Wientjes, I. G. M. & van den Berg, J. 2007*a* Grain sorting over offshore sandwaves: observations and modelling. In *Fifth IAHR Symp. on River, Coastal and Estuarine Morphodynamics*, 17–21 September 2007, University of Twente, The Netherlands.

Roos, P. C., Wemmenhove, R., Hulscher, S. J. M. H., Hoeijmakers, H. W. M. & Kruyt, N. O. 2007*b* Modeling the effect of non-uniform sediment on the dynamics of offshore tidal sand banks. *J. Geophys. Res.* **112**, F02011, doi:10.1029/2005JF000376.

Schüttenhelm, R. T. E. 2002 Grain-sorting variability and crest stability of a North Sea sand wave in space and time. *TNO Rep.* 02-219-B. Netherlands Institute of Apllied Geosciences, Utrecht, The Netherlands.

Seminara, G. 1998 Stability and morphodynamics. *Meccanica* **33**, 59–99.

Soulsby, R. L. & Whitehouse, J. S. 2005 Prediction of ripple properties in shelf seas *Tech. Rep.* 154. Wallingford Ltd.

Stuart, J. T. 1966 Double boundary layers in oscillatory viscous flow. *J. Fluid Mech.* **24**, 673–687.

Swift, D. J. P., Parker, G., Lanfredi, N. W., Perillo, G. & Figge, K. 1978 Shoreface-connected sand ridges on American and European shelves: a comparison. *Estur. Coast. Mar. Sci.* **7**, 257–273.

Ten Brummelhuis, P. G. J., Gerritsen, H. & Van der Kaay, T. 1997 Sensitivity analysis and calibration of the orthogonal boundary-fitted coordinate model PROMISE for tidal flow: the use of adjoint modelling techniques. *Res. Rep.* Z2025. Delft Hydraulics, Delft, The Netherlands.

Terwindt, J. H. J. 1971 Sand waves in the Southern bight of the North Sea. *Mar. Geology*. **10**, 51–67.

Van Lancker, V. R. M. & Jacobs, P. 2000 The dynamical behaviour of shallow marine dunes. In *International Workshop on Marine Sandwave Dynamics*, 23–24 March (ed. A. Trentesaux & T. Garlan), University of Lille I.

Van Lancker, V. R. M. 1999 Sediment and morphodynamics of a siliciclastic near coastal area, in relation to hydrodynamical and meteorological conditions: Belgian continental shelf. *PhD thesis*, Gent University, Belgium.

Van Rijn, L. C. 1991 Sediment transport in combined waves and currents. In *Proceedings of Euromech 262*, Balkema.

van der Veen, H. H. 2008 Natural and human induced seabed evolution. *PhD thesis*, University of Twente, The Netherlands.

Vincent, C. E., Stolk, A. & Porter, C. F. C. 1998 Sand suspension and transport on the Middelkerke Bank (southern North Sea) by storms and tidal currents. *Mar. Geol.***150**, 113–129.

Walgreen, M., de Swart, H. E. & Calvete, D. 2004 A model for grain-sorting over tidal sand ridges. *Ocean Dyn.* **54**, 374–384.